

Analysis of azimuthal magnetorotational instability and Tayler instability of rotating MHD flows via an extended Hain-Lüst equation

R. Zou

Zhejiang Normal University, 688 Yingbin Road, Jinhua, Zhejiang, 321004, China

J. Labarbe and O. N. Kirillov

Northumbria University, Newcastle upon Tyne, NE1 8ST, UK

Y. Fukumoto

Institute of Mathematics for Industry, Kyushu University, Fukuoka, 819-0395, Japan

(Dated: December 21, 2024)

Short-wavelength local analysis and numerical global analysis are made of the azimuthal magnetorotational instability of rotating flows of an electrically conducting fluid, subject to an arbitrary but axisymmetric azimuthal magnetic field, to three-dimensional disturbances. We extend the Hain-Lüst equation for the radial Lagrangian displacements by incorporating the effect of the viscosity and electrical resistivity and apply the Wentzel-Kramers-Brillouin method to it. We confirm that in the inductionless limit, in which the magnetic diffusivity is much larger than the viscosity, rotating flows with radial distributions of the angular velocity beyond the Liu limit, become unstable subject to a wide variety of the azimuthal magnetic fields, and so is the Keplerian flow. Our results compare well with the numerical global stability analysis.

I. INTRODUCTION

Since the rediscovery of Velikhov's [1] and Chandrasekhar's [2] result by Balbus and Hawley [3], the magnetorotational instability (MRI) has aroused strong interest as a promising mechanism for triggering turbulence in the flow of an accretion disk and for promoting outward transport of angular momentum, while the matter accretes to the center. For an accretion disk, the Keplerian flow, a cylindrically symmetric flow with the profile $U_\theta \propto r^{-1/2}$ of rotational velocity, satisfies the force balance: $U_\theta^2(r)/r = \Omega^2(r)r = -\nabla\Phi$; $\Phi \propto 1/r$. Here r is the distance from the axis of symmetry. A combined effect of fluid rotation and the imposed axial magnetic field makes unstable the Keplerian flow of an ideal conducting fluid, for which the fluid viscosity and the electric resistivity are neglected.

Let us introduce the cylindrical coordinates (r, θ, z) with the z -axis along the axis of symmetry, along with $\mathbf{e}_r, \mathbf{e}_\theta$ and \mathbf{e}_z being the unit vectors in the radial, azimuthal, and axial direction, respectively. A steady rotating flow with the angular velocity $\Omega(r)\mathbf{e}_z$, parallel to the z -axis is considered as a base state. The Rossby number is defined [4, 5] by $Ro = 1/2(d \log \Omega / d \log r) = r\Omega'/(2\Omega)$, where the prime designates the derivative with respect to r . Without loss of generality, we assume that $\Omega > 0$. For a non-magnetized flow, Rayleigh's criterion states that the instability with respect to axisymmetric disturbance occurs when the Rossby number, $Ro < -1$, which fails to include the Keplerian flow ($Ro = -3/4$). When magnetic field acts, the axial or the azimuthal magnetic field raises the critical Rossby number from -1 to zero [1, 2] and near zero [6–8] respectively, so that the Keplerian flow is turned into unstable. The former is the standard MRI (SMRI) for which the magnetic field has

only the axial component $\mathbf{B} = B_z\mathbf{e}_z$. The latter is called the azimuthal MRI (AMRI), for which the magnetic field has only the azimuthal component $\mathbf{B} = B_\theta(r)\mathbf{e}_\theta$. The instability caused by their combination is called the helical MRI (HMRI) [4, 5, 9].

In a protoplanetary disk surrounding a young star, the ionization depends on the radiation from the X-rays and cosmic rays [10], and the temperature of the disk. The mid-plane of the accretion disk receives fewer radiation and the cold region of the disk is only weakly ionized. Laboratory experiments with rotating plasma such as the Madison plasma Couette flow experiment (MPCX) [11] and with the Taylor-Couette flow of liquid metals (sodium, gallium, and liquid eutectic alloy $Ga^{67}In^{20.5}Sn^{12.5}$) such as the Potsdam Rossendorf Magnetic Instability Experiment (PROMISE) [4] were designed for detecting the MRI [12, 13]. For the cold and less radiated parts of the protoplanetary and accretion disks as well as for the experiments with liquid metals, the effects of both the viscosity ν and the magnetic diffusivity η are not ignorable. Because of the low electric conductivity, the magnetic Prandtl number $Pm = \nu/\eta$ is very small [14] (e.g. $Pm \sim 10^{-5}$ for liquid sodium, $Pm \sim 10^{-6}$ for gallium and liquid eutectic alloy $Ga^{67}In^{20.5}Sn^{12.5}$). The case of $\nu/\eta \ll 1$ is referred to as the inductionless limit [4, 9]. By contrast, in the hot parts of the accretion disks, because of the high electric conductivity, Pm can become very large, see e.g. [15] where Pm ranges from 10^{-3} to 10^3 .

Given an axial magnetic field at some instant, the radial component is seeded by perturbing the axial field. Once the radial component arises, with the magnetic field frozen into the fluid, the radial component is tilted by the differential rotation to produce azimuthal component, and the latter component is constantly stretched with time, resulting in establishing a strong azimuthal

component [16]. In reality, three-dimensional numerical simulations demonstrated that the initial weak azimuthal magnetic field tends to be stretched out to become, at a later stage, dominant over the initial axial magnetic field [17, 18]. Hence, it is worthwhile to look into the instability of a rotating flow caused by the applied azimuthal magnetic field (AMRI) [6–8, 17, 19–21] and by the combination of the azimuthal and the axial magnetic field (HMRI) [4, 22–24].

The HMRI and the AMRI in the inductionless limit were addressed for axisymmetric and non-axisymmetric perturbations both numerically and in the short-wavelength regime by traditional Wentzel-Kramers-Brillouin (WKB) method [4, 25] and within the geometrical optics [6] approximation [21, 26–30]. We revisit these inductionless instabilities by a different route. We apply the WKB method to the full linearized equation written in terms of the radial Lagrangian displacement, i.e. to the Hain-Lüst equation [31, 32] augmented with the dissipation and the magnetic diffusion terms to be derived here, rather than to the equations of magnetohydrodynamics (MHD) in their original form. We derive the dispersion relation similar to the previously known one [25, 29, 30], but augmented with a few more terms that will enable us to address the case of small axial wavenumbers in more detail.

As mentioned above, in the ideal MHD limit, the SMRI widens the instability range of the Rayleigh’s centrifugal instability ($Ro < -1$) up to the solid body rotation ($Ro < 0$). Connection of the two criteria requires taking into account viscosity and electrical conductivity of the fluid [33–35]. For the azimuthal and helical MRI, however, the instability criterion is sensitive to the magnetic shear [29, 30]. The WKB analysis can handle general magnetic shear characterized by the magnetic Rossby number [29] $Rb = r^2(B_\theta/r)/(2B_\theta)$, though many of the previous studies were restricted to $Rb = -1$, correspondingly to $B_\theta \propto r^{-1}$, being called the current-free field [4, 6, 7, 26].

An axisymmetric analysis for the HMRI for $Rb = -1$ in the inductionless limit [4, 36] of $Pm \rightarrow 0$ has shown that the critical Rossby number is raised from the Rayleigh value $Ro = -1$ to the lower Liu limit [30, 36] $Ro = 2(1 - \sqrt{2}) \approx -0.8284$, which is smaller than the critical value $Ro = 0$ for the ideal SMRI. The Liu limit is attained [26, 30] at $B_\theta/B_z = 1/\sqrt{2}$. Hence, the inductionless HMRI excludes the Keplerian flow of $Ro = -3/4$. Even if non-axisymmetric disturbances are taken into account, the critical Ro remains to be the Liu limit [26]. The same holds for the inductionless AMRI [21, 26, 30].

Recently it was discovered that, if the magnetic profile is made slightly shallower than $B_\theta \propto r^{-1}$, so as to satisfy the condition $Rb \geq -25/32$, the Keplerian flow invites both the inductionless AMRI and HMRI [21, 29, 30]. Later on, these results were confirmed numerically [37].

In the work on the short-wavelength stability analysis of the AMRI of an ideal MHD, Zou and Fukumoto [8] proposed a new approximation scheme. In it, one

first deduces a differential equation for the radial component of the displacement field, or the Hain-Lüst equation [31, 32], derivable from the Frieman-Rosenbluth equation [31, 32, 38], and thereafter substitutes the WKB form of the radial solution into the result. In the present paper we apply this idea to the case of the non-ideal MHD. The extended Hain-Lüst equation, incorporating effects of both the viscosity and resistivity, serves as a basis for the linear stability analysis of the AMRI and HMRI both in the inductionless limit of $Pm \rightarrow 0$ and in the case of general Pm and Rb .

The problem is formulated in Section II. By performing the WKB analysis of the extended Hain-Lüst equation, we obtain the dispersion relation in the short radial wavelength limit in Section III. Section IV confirms that this approach restores the known results [4, 5] for the SMRI and the AMRI, when restricted to axisymmetric disturbances.

In Section V, we focus on the non-axisymmetric AMRI. We will see that in the weak magnetic field limit, the Rayleigh criterion decides the instability. Then we proceed to the case of sufficiently strong azimuthal magnetic field. We deal exclusively with two extreme modes of $kr \rightarrow 0$ and $kr \rightarrow \infty$, being featured by the axial wavenumber k . For the Keplerian flow, the short axial-wavelength mode ($kr \rightarrow \infty$) is excitable for $Rb > -25/32$, in accordance with the earlier works [29, 30]. We find that the long axial-wavelength mode ($kr \rightarrow 0$) is excitable for $Rb < -1/4$ even when the flow is non-rotating. The growth rate of the both modes is proportional to the square of the field strength.

The local analysis disregards the boundary conditions. However, it turns out that in the limit of $kr \rightarrow 0$, an upper limit of the value of qr , where q is the radial wavenumber, is placed for the instability to occur. In Section VI, we analyse numerically our WKB dispersion relation with a reasonable restriction on the radial wavenumber q . This results in the stability diagrams well compared with that of the global numerical analysis of the work [39] and local analysis of the works [27, 30] for various values of the magnetic Prandtl number.

Finally, in section VII we complement the local stability analysis with the global stability analysis of the original MHD system equipped with boundary conditions that we solve by the pseudo-spectral method [40–42] to validate the theory.

II. EXTENDED HAIN-LÜST EQUATION

We consider the linear stability of a cylindrically symmetric rotating flow, of an incompressible viscous fluid with finite electric conductivity, to three-dimensional disturbances. The basic state is a rotating flow in equilibrium with the velocity field $\mathbf{U} = \mathbf{U}(r)$, characterized by the angular velocity $\Omega(r)$, in the externally imposed steady magnetic field $\mathbf{B} = \mathbf{B}(r)$, of the same symmetry, with the azimuthal and the axial components $r\mu(r)$ and

$B_z(r)$, respectively:

$$\mathbf{U} = r\Omega(r)\mathbf{e}_\theta, \quad \mathbf{B} = r\mu(r)\mathbf{e}_\theta + B_z\mathbf{e}_z, \quad (1)$$

where the axial component B_z is assumed to be constant.

The velocity \mathbf{u} , the magnetic field \mathbf{b} and the total pressure p are partitioned into the basic flow, and the disturbance as

$$\mathbf{u} = \mathbf{U} + \tilde{\mathbf{u}}, \quad \mathbf{b} = \mathbf{B} + \tilde{\mathbf{b}}, \quad p = P + \tilde{p}. \quad (2)$$

The Navier-Stokes and the induction equations linearized in the disturbance $(\tilde{\mathbf{u}}, \tilde{\mathbf{b}}, \tilde{p})$ are

$$\begin{aligned} \frac{\partial \tilde{\mathbf{u}}}{\partial t} + (\tilde{\mathbf{u}} \cdot \nabla)\mathbf{U} + (\mathbf{U} \cdot \nabla)\tilde{\mathbf{u}} &= -\frac{1}{\rho}\nabla\tilde{p} \\ &+ \frac{1}{\rho\mu_0}(\mathbf{B} \cdot \nabla)\tilde{\mathbf{b}} + \frac{1}{\rho\mu_0}(\tilde{\mathbf{b}} \cdot \nabla)\mathbf{B} + \nu\nabla^2\tilde{\mathbf{u}}, \end{aligned} \quad (3)$$

$$\frac{\partial \tilde{\mathbf{b}}}{\partial t} = \nabla \times (\mathbf{U} \times \tilde{\mathbf{b}}) + \nabla \times (\tilde{\mathbf{u}} \times \mathbf{B}) + \eta\nabla^2\tilde{\mathbf{b}}, \quad (4)$$

$$\nabla \cdot \tilde{\mathbf{u}} = 0, \quad (5)$$

$$\nabla \cdot \tilde{\mathbf{b}} = 0, \quad (6)$$

where μ_0 , ν and η represent the magnetic permeability, the kinematic viscosity and the magnetic diffusivity, respectively. We assume that μ_0 , ν , η are all constant [21].

Owing to the steadiness and to the symmetries with respect to translation along and rotation about the z -axis, we may pose the disturbances in the normal-mode form $\exp[\lambda t + i(m\theta + kz)]$. The azimuthal wavenumber m takes an integer value, the axial wavenumber k is taken to be a real number, and λ is the eigenvalue to be calculated. Substitution of this normal-mode form into (3)–(6) yields a coupled system of 8 ordinary differential equations for functions of r .

The viscous and the resistive terms stand as obstacles to carry through the stability analysis. With a view to incorporate only the leading-order effect of short-wave radial disturbances under the assumption of ν and η being small, we may simply replace $-\nabla^2$ with $|\mathbf{k}|^2 = k^2 + q^2 + m^2/r^2$ and introduce the radial wavenumber $q(r)$. This procedure amounts to discarding the terms including the derivative of $q(r)$ and m/r , and should be justified *a posteriori*. The resulting equations are combined into matrix form for the vector of variables $\boldsymbol{\xi} = (\tilde{u}_r, \tilde{u}_\theta, \tilde{u}_z, \tilde{b}_r, \tilde{b}_\theta, \tilde{b}_z, \tilde{p})$ as

$$\mathbf{M}\boldsymbol{\xi} = 0 \quad (7)$$

with

$$\mathbf{M} = \begin{pmatrix} \tilde{\lambda}_\nu & -2\Omega & 0 & -\frac{iF}{\rho\mu_0} & \frac{2\mu}{\rho\mu_0} & 0 & \frac{1}{\rho}\frac{d}{dr} \\ \frac{1}{r}\frac{d}{dr}(r^2\Omega) & \tilde{\lambda}_\nu & 0 & -\frac{2\mu + r\frac{d\mu}{dr}}{\rho\mu_0} & -\frac{iF}{\rho\mu_0} & 0 & \frac{1}{\rho}im \\ 0 & 0 & \tilde{\lambda}_\nu & 0 & 0 & -\frac{iF}{\rho\mu_0} & \frac{r\rho}{\rho} \\ -iF & 0 & 0 & \tilde{\lambda}_\eta & 0 & 0 & 0 \\ r\frac{d\mu}{dr} & -iF & 0 & -r\frac{d\Omega}{dr} & \tilde{\lambda}_\eta & 0 & 0 \\ 0 & 0 & -iF & 0 & 0 & \tilde{\lambda}_\eta & 0 \\ \frac{1}{r} + \frac{d}{dr} & \frac{im}{r} & ik & 0 & 0 & 0 & 0 \\ 0 & 0 & 0 & \frac{1}{r} + \frac{d}{dr} & \frac{im}{r} & ik & 0 \end{pmatrix}, \quad (8)$$

where $F = m\mu + B_z k$, $\tilde{\lambda}_\nu = \lambda + im\Omega + \omega_\nu$, $\tilde{\lambda}_\eta = \lambda + im\Omega + \omega_\eta$, $\omega_\nu = |\mathbf{k}|^2\nu$, and $\omega_\eta = |\mathbf{k}|^2\eta$.

We reduce the coupled system of the ordinary differential equations (7) to a single ordinary differential equation governing the radial Lagrangian displacement of a fluid particle. The details of the derivation is relegated to Appendix A.

For the ideal MHD, the vorticity and the magnetic field are both frozen into the fluid and the Lagrangian variable helps to construct the iso-magnetovortical [43] perturbations, with respect to which the stability analysis is typically made. This is no longer true for the non-ideal case. We find that, with ν and η included, the following ‘quasi’ radial displacement $\xi_r = u_r/\tilde{\lambda}_\eta$, connected with the radial component \tilde{u}_r , is advantageous for simplifying the resulting equation. This differs from the radial Lagrangian displacement by the ω_η term in $\tilde{\lambda}_\eta$.

We introduce a new dependent variable $\chi = -ru_r/\tilde{\lambda}_\eta$, with the minus sign chosen for convenience, and the following notation

$$\Lambda = \tilde{\lambda}_\nu + \frac{F^2}{\tilde{\lambda}_\eta\rho\mu_0}, \quad (9)$$

$$h^2 = k^2 + m^2/r^2. \quad (10)$$

With this, the system (7) collapses into a single second-order ordinary differential equation for $\chi(r)$

$$\frac{d}{dr}\left(f\frac{d\chi}{dr}\right) + s\frac{d\chi}{dr} - g\chi = 0, \quad (11)$$

where

$$\begin{aligned} f &= \frac{\tilde{\lambda}_\eta\Lambda}{h^2r}, \quad s = \frac{imE(\tilde{\lambda}_\nu - \tilde{\lambda}_\eta)}{h^2r}\Omega', \\ g &= \frac{d}{dr}\left[\frac{im\tilde{\lambda}_\eta}{h^2r^2}\left(\left(1 - \frac{\tilde{\lambda}_\nu}{\tilde{\lambda}_\eta}\right)r\Omega' + 2\left(\Omega - \frac{iF\mu}{\rho\mu_0\tilde{\lambda}_\eta}\right)\right)\right] \\ &+ \frac{E\tilde{\lambda}_\eta}{\Lambda r} - \left(\Omega - \frac{iF\mu}{\rho\mu_0\tilde{\lambda}_\eta}\right) \\ &\times \frac{2m^2\tilde{\lambda}_\eta}{\Lambda h^2r^3}\left[\left(1 - \frac{\tilde{\lambda}_\nu}{\tilde{\lambda}_\eta}\right)r\Omega' + 2\left(\Omega - \frac{iF\mu}{\rho\mu_0\tilde{\lambda}_\eta}\right)\right], \end{aligned} \quad (12)$$

with the prime denoting the derivative with respect to r . The expression for the coefficient E is given by the formula (A4) in the Appendix A.

This is thought of as a version of the Hain-Lüst equation [31] extended with allowance for the effect of viscous dissipation and magnetic diffusion. When $\nu = 0$ and $\eta = 0$, (11) and (12) reduce to the well-known Hain-Lüst equation of the ideal MHD [8, 31].

III. DISPERSION RELATION IN SHORT RADIAL WAVELENGTH APPROXIMATION

We apply the WKB approximation [31] to (11) by introducing the ansatz $d\chi/dr = c(r) \exp\{i \int q(r) dr\}$ and assuming that the radial wavelength is very short, i.e. $q(r)L \gg 1$, where L is the length scale for the radial inhomogeneity. This results in the algebraic dispersion equation

$$\begin{aligned} & (h^2 + q^2)\tilde{\lambda}_\eta^2 \Lambda^2 + 4k^2 \left(\Omega \tilde{\lambda}_\eta - \frac{iF\mu}{\rho\mu_0} \right) \\ & \times \left[\Omega Ro(\omega_\eta - \omega_\nu) + \left(\Omega \tilde{\lambda}_\eta - \frac{iF\mu}{\rho\mu_0} \right) \right] \\ & + 4\Lambda h^2 \tilde{\lambda}_\eta \left[\left(\Omega^2 Ro - \frac{\mu^2}{\rho\mu_0} Rb \right) + \frac{imr}{2} \frac{d}{dr} \left(\frac{\Omega \tilde{\lambda}_\eta - \frac{i\mu F}{\rho\mu_0}}{h^2 r^2} \right) \right] \\ & = 0, \end{aligned} \quad (13)$$

where we have introduced the Rossby number Ro and the magnetic Rossby number Rb by [26, 29, 30]

$$Ro = \frac{1}{2} \frac{r}{\Omega} \Omega', \quad Rb = \frac{1}{2} \frac{r}{\mu} \mu'. \quad (14)$$

In the ideal case when $\omega_\nu = 0$ and $\omega_\eta = 0$ the dispersion relation (13) reduces to that of the work [8] that, in its turn reduces to the ideal dispersion relation derived by Ogilvie and Pringle [7] and Friedlander and Vishik [6] as well as to the ideal versions of the dispersion relation of the works [25, 29, 30] in the limit of large axial wavenumbers, $k \rightarrow \infty$.

Applying the WKB approximation to the extended Hain-Lüst equation for the radial Lagrangian displacement rather than to the coupled system of the ordinary differential equations (7) we obtain an additional term $\frac{imr}{2} \left(\frac{1}{h^2 r^2} (\Omega \tilde{\lambda}_\eta - \frac{i\mu F}{\rho\mu_0}) \right)'$ in the resulting dispersion relation (13). We notice that the axisymmetric mode ($m = 0$) remains intact since this term is irrelevant. However, it can improve the prediction accuracy in the case of non-axisymmetric perturbations with long axial wavelength.

For our purpose of stability analysis, it is expedient to define two kinds of Alfvén frequency ω_A and $\omega_{A\theta}$, along with their ratio β representing the helical geometry of the magnetic field, by [30]

$$\omega_A = \frac{kB_z}{\sqrt{\rho\mu_0}}, \quad \omega_{A\theta} = \frac{\mu}{\sqrt{\rho\mu_0}}, \quad \beta = \frac{\omega_{A\theta}}{\omega_A}. \quad (15)$$

In addition, we introduce three dimensionless parameters, namely, the magnetic Prandtl number Pm , the Reynolds number Re and the Hartmann number Ha by [30]

$$Pm = \frac{\omega_\nu}{\omega_\eta}, \quad Re = \frac{\Omega}{\omega_\nu}, \quad Ha = \frac{\omega_A}{\sqrt{\omega_\nu \omega_\eta}}. \quad (16)$$

The dispersion relation for non-dimensional variables, with the derivative term in (13) being expanded out, leads to

$$\begin{aligned} & (\Lambda_1 \Lambda_2 + \widehat{Ha}^2)^2 \\ & + 4 \frac{\widehat{h}^2 (\Lambda_1 \Lambda_2 + \widehat{Ha}^2)}{\widehat{h}^2 + \widehat{q}^2} (Re^2 Pm Ro - \beta^2 Ha^2 Rb) \\ & + \frac{4im(\Lambda_1 \Lambda_2 + \widehat{Ha}^2)}{\widehat{h}^2 + \widehat{q}^2} \left[Re Ro \sqrt{Pm} (\Lambda_2 + im Re \sqrt{Pm}) \right. \\ & \left. - i(2m\beta + 1)\beta Ha^2 Rb + (i\widehat{Ha}\beta Ha - Re \sqrt{Pm} \Lambda_2) \frac{\widehat{k}^2}{\widehat{h}^2} \right] \\ & + 4\alpha^2 \left[(Re \Lambda_2 \sqrt{Pm} - i\widehat{Ha}\beta Ha) (Re \Lambda_2 \sqrt{Pm} - i\widehat{Ha}\beta Ha \right. \\ & \left. + Ro Re(1 - Pm)) \right] = 0, \end{aligned} \quad (17)$$

where

$$\begin{aligned} \Lambda_1 &= \frac{\lambda}{\Omega} Re \sqrt{Pm} + im Re \sqrt{Pm} + \sqrt{Pm}, \\ \Lambda_2 &= \frac{\lambda}{\Omega} Re \sqrt{Pm} + im Re \sqrt{Pm} + \frac{1}{\sqrt{Pm}}, \\ \widehat{Ha} &= Ha(1 + m\beta), \\ \widehat{k} &= kr, \quad \widehat{q} = qr, \quad \widehat{h} = hr, \quad \alpha^2 = \frac{\widehat{k}^2}{\widehat{h}^2 + \widehat{q}^2}. \end{aligned} \quad (18)$$

In the rest of the paper, this form of the dispersion relation plays the decisive role for determining the instability criteria and for calculating the growth rates.

IV. AXISYMMETRIC PERTURBATIONS IN THE INDUCTIONLESS LIMIT

To begin with, we confirm that (17) and (18) reproduce the known results in the axisymmetric case. For the axisymmetric SMRI ($m = 0$, $\mathbf{B} = B_z \mathbf{e}_z$), the dispersion relation (17) simplifies, in the inductionless limit ($Pm \rightarrow 0$), to

$$4\alpha^2 Re^2 (1 + Ro) + (1 + Ha^2 + \frac{\lambda}{\Omega} Re)^2 = 0. \quad (19)$$

The growth rate can be solved from (19) as

$$\frac{\lambda}{\Omega} = -\frac{1 + Ha^2}{Re} \pm 2\sqrt{-\alpha^2(1 + Ro)}, \quad (20)$$

where $\alpha^2 = \widehat{k}^2/(\widehat{q}^2 + \widehat{k}^2)$ when $m = 0$, see (18). From (20), the instability region is [4]

$$Ro < Ro_c = -1 - \left(\frac{1 + Ha^2}{2\alpha Re} \right)^2. \quad (21)$$

As Re goes to infinity the critical Rossby number approaches $Ro_c = -1$. Here the magnetic field lowers the critical Rossby number. This is different from ideal SMRI where magnetic field, no matter how weak it may be, can raise the critical Rossby number from $Ro_c = -1$ for hydrodynamic flows to $Ro_c = 0$ for MHD flows, which is known as the Velikhov-Chandrasekhar paradox [34, 35, 44]. The viscosity acts to stabilize the MHD flow when the axial magnetic field B_z is weak.

Next, we consider the inductionless azimuthal MRI (AMRI), where the magnetic field has only the azimuthal component $\mathbf{B} = r\mu(r)\mathbf{e}_\theta$. Let

$$Ha_\theta = \frac{\omega_{A\theta}}{\sqrt{\omega_\nu\omega_\eta}} \quad (22)$$

be the azimuthal Hartmann number. Then, based on the definition (15) for β we can write $\beta = Ha_\theta/Ha$ and use this expression in the dispersion relation (17). Putting $m = 0$ in (17) and then taking the limit $Ha \rightarrow 0$, we obtain the dispersion relation for the pure azimuthal magnetic field that in the inductionless limit of $Pm \rightarrow 0$ yields [30]

$$\frac{\lambda}{\Omega} = \frac{-1 + 2\alpha^2 Ha_\theta^2 Rb \pm 2\alpha \sqrt{\alpha^2 Ha_\theta^4 Rb^2 - (1 + Ro)Re^2}}{Re}. \quad (23)$$

Its behavior at large values of Re is

$$\frac{\lambda}{\Omega} \approx 2i\alpha\sqrt{1 + Ro} + (2\alpha^2 Ha_\theta^2 Rb - 1)\frac{1}{Re} \quad (24)$$

When $Re \rightarrow \infty$, simple instability conditions are read off from the zeroth- and the first-order coefficients of (23) as

$$\begin{aligned} Ro &< -1, \text{ arbitrary value of } Rb \\ Ro &\geq -1, Rb > \frac{1}{2\alpha^2 Ha_\theta^2}. \end{aligned} \quad (25)$$

In the rest of this section, we revisit the axisymmetric ($m = 0$) HMRI occurring in the presence of both azimuthal and axial components of the magnetic field $\mathbf{B} = r\mu(r)\mathbf{e}_\theta + B_z\mathbf{e}_z$. The dispersion relation (17) is solved for the eigenvalue as [30]

$$\begin{aligned} \frac{\lambda}{\Omega} = & -\frac{1}{Re} + \frac{Ha^2}{Re}(2\alpha^2\beta^2 Rb - 1) \\ & \pm \frac{2\alpha}{Re} [\beta^2 Ha^4(1 + \alpha^2\beta^2 Rb^2) - Re^2(1 + Ro) \\ & + i\beta Ha^2 Re(2 + Ro)]^{1/2}. \end{aligned} \quad (26)$$

At large values of Re , (26) is expanded as

$$\begin{aligned} \frac{\lambda}{\Omega} &\approx \pm 2i\alpha\sqrt{1 + Ro} + \left[-1 + Ha^2(2\alpha^2\beta^2 Rb - 1 \right. \\ &\quad \left. \pm \frac{(2 + Ro)\alpha\beta}{\sqrt{1 + Ro}} \right] \frac{1}{Re}, \quad (Ro \neq -1), \\ \frac{\lambda}{\Omega} &\approx \pm 2\alpha Ha \sqrt{i\beta} \frac{1}{\sqrt{Re}} + (-1 - Ha^2 + 2\alpha^2\beta^2 Ha^2 Rb) \frac{1}{Re}, \\ &\quad (Ro = -1). \end{aligned} \quad (27)$$

From the zeroth-order term in (27), $Ro < -1$ is sufficient for instability and so is $Ro = -1$ unless $Ha = 0$ or $\beta = 0$. The remaining task is classification for the case of $Ro > -1$. Equation (27) tells that the growth rate, if it is positive, increases with $|Ha|$.

For $1 \ll Ha \ll Re$ and $Ro \neq -1$, (27) reads for the growth rates [30]

$$\frac{\Re(\lambda)}{\Omega} = \left(2\alpha^2\beta^2 Rb - 1 \pm \alpha\beta \frac{Ro + 2}{\sqrt{1 + Ro}} \right) N - \frac{1}{Re}, \quad (28)$$

where $N = Ha^2/Re$ is known as the Elsasser number [30] and $\Re(\cdot)$ designates the real part. The coefficient at N is a quadratic equation with respect to $\alpha\beta$. Its discriminant is

$$D = 8Rb + \frac{(Ro + 2)^2}{Ro + 1}.$$

Therefore, for $Rb < 0$ the coefficient at N can be positive, if $D > 0$, which yields [29, 30]

$$Rb > -\frac{1}{8} \frac{(Ro + 2)^2}{Ro + 1} \quad (29)$$

as a necessary condition for instability.

Note that when $Rb < 0$ and $Re \rightarrow \infty$ the maximum of the growth rate, as a function of $\alpha\beta$, turns out to be

$$\frac{\Re(\lambda)}{\Omega} = -\frac{DN}{8Rb}$$

and is attained at

$$\alpha\beta = \mp \frac{Ro + 2}{4Rb\sqrt{Ro + 1}}.$$

Correspondingly, the instability occurs in the region [29, 30]

$$\begin{aligned} Ro \in & \left[-1, 2 \left(-\sqrt{2}\sqrt{2Rb^2 + Rb} - 1 - 2Rb \right) \right] \\ & \cup \left[2 \left(\sqrt{2}\sqrt{2Rb^2 + Rb} - 1 - 2Rb \right), +\infty \right]. \end{aligned} \quad (30)$$

In particular, for $Rb = -1$ the critical Rossby numbers are $Ro_c = 2(1 \pm \sqrt{2})$ at $\alpha\beta = \pm 1/\sqrt{2}$, and thus the upper and lower Liu limits are recovered [4, 5, 36].

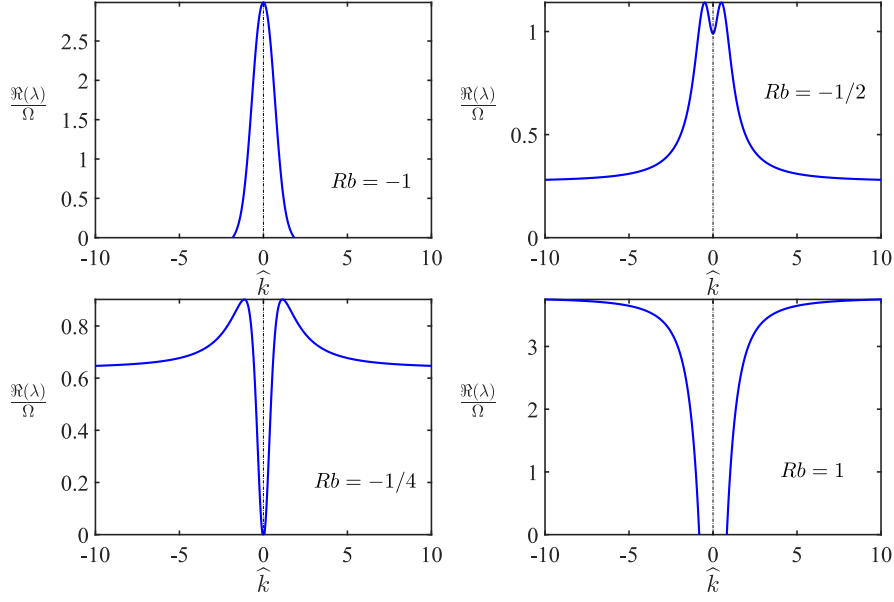


FIG. 1. The growth rate $\Re(\lambda)/\Omega$ versus the dimensionless axial wavenumber $\hat{k} = kr$ in the inductionless approximation (32) for $Re = 100$, $Ha_\theta = 10$, $m = 1$, $\hat{q} = 0$, $Ro = -3/4$. From upper left to lower right, Rb is varied from -1 to 1 . As Rb increases, the value of \hat{k} corresponding to the maximum growth rate increases from $\hat{k} = 0$ to finite but nonzero value and ultimately this $\hat{k} \rightarrow \infty$.

V. NON-AXISYMMETRIC PERTURBATIONS IN THE INDUCTIONLESS LIMIT

Hereafter we limit ourselves to the magnetic field that has the azimuthal component only. We first substitute $\beta = Ha_\theta/Ha$ into (17) and then take the limit $Ha \rightarrow 0$. As a result, we get the dimensionless dispersion relation of AMRI

$$\begin{aligned}
& (\Lambda_1\Lambda_2 + m^2Ha_\theta^2)^2 \\
& + 4\frac{\hat{h}^2(\Lambda_1\Lambda_2 + m^2Ha_\theta^2)}{\hat{h}^2 + \hat{q}^2}(Re^2PmRo - Ha_\theta^2Rb) \\
& + \frac{4im(\Lambda_1\Lambda_2 + m^2Ha_\theta^2)}{\hat{h}^2 + \hat{q}^2}\left[ReRo\sqrt{Pm}(\Lambda_2 + imRe\sqrt{Pm})\right. \\
& \left. - 2imHa_\theta^2Rb + (imHa_\theta^2 - Re\sqrt{Pm}\Lambda_2)\frac{\hat{k}^2}{\hat{h}^2}\right] \\
& + 4\alpha^2\left[(Re\Lambda_2\sqrt{Pm} - imHa_\theta^2)(Re\Lambda_2\sqrt{Pm} - imHa_\theta^2\right. \\
& \left. + RoRe(1 - Pm))\right] = 0. \tag{31}
\end{aligned}$$

Taking the limit of $Pm \rightarrow 0$ in (31), we get

$$\begin{aligned}
& \hat{\lambda}^2 + \frac{4\hat{\lambda}}{\hat{h}^2 + \hat{q}^2}\left\{Ha_\theta^2\left(2m^2Rb - \hat{h}^2Rb - \frac{\hat{k}^2m^2}{\hat{h}^2}\right)\right. \\
& \left. + imRe\left(Ro - \frac{\hat{k}^2}{\hat{h}^2}\right)\right\} \\
& + 4\alpha^2(Re - imHa_\theta^2)(Re - imHa_\theta^2 + ReRo) = 0, \tag{32}
\end{aligned}$$

where

$$\hat{\lambda} = 1 + Ha_\theta^2m^2 + \frac{\lambda Re}{\Omega} + imRe.$$

Note that at $m = 0$ the roots of the dispersion relation (32) reduce to (23).

A. Weak field

To examine the instability when magnetic field is weak, we express the solution of (32) in powers of small parameter Ha_θ . Then its leading-order term reads

$$\begin{aligned}
\frac{\lambda}{\Omega} = & -\frac{1}{Re} - im\left[1 + \frac{2}{\hat{h}^2 + \hat{q}^2}\left(Ro - \frac{\hat{k}^2}{\hat{h}^2}\right)\right] \\
& \pm 2\sqrt{-\alpha^2(1 + Ro) - \frac{m^2}{(\hat{h}^2 + \hat{q}^2)^2}\left(Ro - \frac{\hat{k}^2}{\hat{h}^2}\right)^2} \\
& + O(Ha_\theta). \tag{33}
\end{aligned}$$

The radicand should be positive in total for instability. The first term in the radicand $-\alpha^2(1 + Ro)$ becomes positive for $Ro < -1$ and the second one is definitely non-positive. This non-positive term has the effect of decreasing the growth rate. If we set $m = 0$ in (33), we get the same result as in (24), except for $o(Ha_\theta)$ terms

$$\frac{\lambda}{\Omega} = \pm 2\alpha i\sqrt{1 + Ro} - \frac{1}{Re}. \tag{34}$$

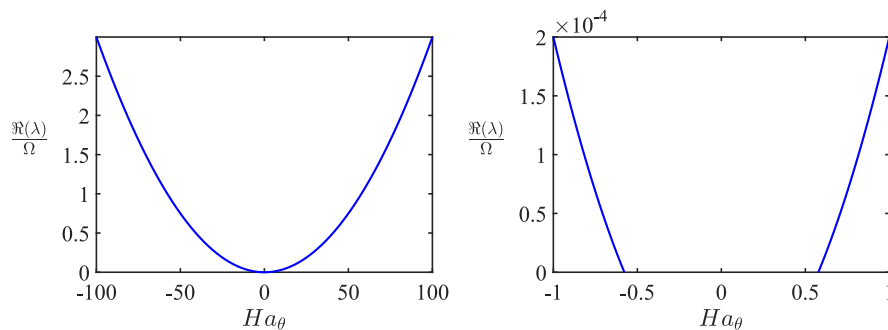


FIG. 2. The growth rate $\Re(\lambda_2)$ of (35) versus Ha_θ when $Re = 10^4$, $m = 1$, $\hat{k} = \hat{q} = 0$, $Ro = -3/4$ and $Rb = -1$. The right panel is the close-up view of the left one near $Ha_\theta = 0$, demonstrating a certain strength of magnetic field needed for instability.

From (34) it follows that instability requires [30]

$$Ro < Ro_c = -1 - \frac{1}{4\alpha^2 Re^2}.$$

Compared with the ideal hydrodynamics, for which the critical Rossby number is $Ro_c = -1$, the critical Rossby number is lowered by $1/(4\alpha^2 Re^2)$ and the maximum growth rate is decreased by $1/Re$ due to viscosity.

When $Ro > -1$, to which the Keplerian flow ($Ro = -3/4$) belongs, the nonaxisymmetric as well as the axisymmetric modes decay as $\lambda/\Omega \approx -1/Re$.

B. Strong field

We turn to the case of a strong magnetic field. The Reynolds number is assumed to be large. The axial wavenumber \hat{k} is an important parameter for determining the maximum growth rate and the instability region.

FIG. 1 shows the growth rate given by equation (32) as a function of \hat{k} for different values of Rb . We fix $m = 1$, $Ro = -3/4$ and $\hat{q} = 0$, because numerically the modes of $\hat{q} = 0$ exhibit the fastest growth. We observe that at around $Rb = -1/4$, there is some finite \hat{k} at which the growth rate takes the maximum value. When Rb is smaller than $-1/4$, the fast growth rate gives way to the $\hat{k} = 0$ mode at $Rb = -1$. When Rb is increased above $-1/4$ by a certain amount, the maximum growth rate is attained in the limit of $\hat{k} \rightarrow \infty$.

1. The limit $\hat{k} \rightarrow 0$

The observations described above suggest us to examine closer the limit of $\hat{k} \rightarrow 0$, which means letting $\alpha \rightarrow 0$ and $\hat{h} \rightarrow m$ in (32). In this limit the roots of (32) at

$Re \gg 1$ take the form

$$\begin{aligned} \frac{\lambda_1}{\Omega} &= -im - (1 + Ha_\theta^2 m^2) \frac{1}{Re}, \\ \frac{\lambda_2}{\Omega} &= -im \left(1 + \frac{4Ro}{m^2 + \hat{q}^2} \right) \\ &\quad - \left[1 + Ha_\theta^2 m^2 \left(1 + \frac{4Rb}{m^2 + \hat{q}^2} \right) \right] \frac{1}{Re}. \end{aligned} \quad (35)$$

A glance at (35) shows that the axisymmetric mode ($m = 0$) is excluded from the unstable ones and the growth rate $\Re(\lambda_1)$ is always negative. The growth rate $\Re(\lambda_2)$ is positive provided that

$$Rb < -\frac{1}{4}(m^2 + \hat{q}^2) \text{ and } Ha_\theta^2 > \frac{1}{m^2 \left(\frac{4|Rb|}{m^2 + \hat{q}^2} - 1 \right)}. \quad (36)$$

FIG. 2 displays the growth rate $\Re(\lambda_2)$ as a function of Ha_θ when $Re = 10^4$, $m = 1$, $\hat{k} = \hat{q} = 0$, $Ro = -3/4$ and $Rb = -1$. The left panel shows that the growth rate increases with Ha_θ ; the right panel is the close-up view near the origin. We recognize that the small but nonzero value $|Ha_\theta| = 1/\sqrt{3} \approx 0.5774$ is necessary for the onset of instability.

Note that rather than Ro , it is now Rb that is tied with the instability and the negative value of $d\mu/dr$ is required. The maximum growth rate is attained at $\hat{q} = 0$.

When $Rb = -1$, the $m = \pm 1$ modes are the only possible modes for instability.

When $m = \pm 1$ is fixed, $Rb < -1/4$ is necessary for the instability of the $\hat{k} = 0$ mode.

It is remarkable that the instability exists, beyond the restriction of the Liu limit, for arbitrary Rossby number Ro . However we should be cautious about this result, because the modes of $\hat{q} = 0$ lie outside the regime of validity of the radial WKB approximation. Later in the article, we argue about the limitation on \hat{q} .

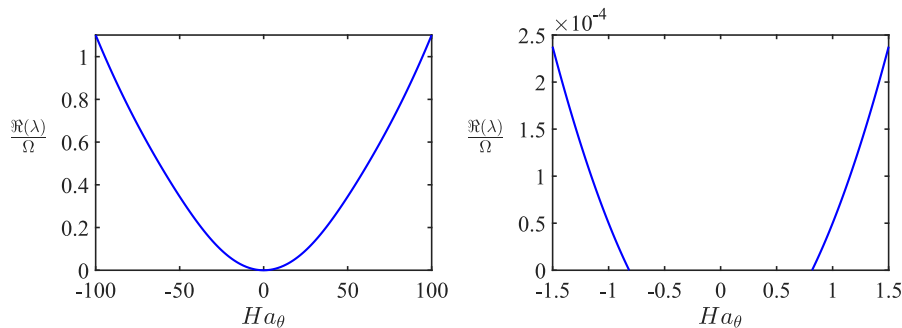


FIG. 3. The growth rate $\Re(\lambda)$ to Ha_θ when $Re = 10^4$, $m = 1$, $\hat{k} \rightarrow \infty$, $Ro = -3/4$ and $Rb = 0$ according to (37). The left panel shows that large Ha_θ increase the growth rate and the right panel is the amplification of the left one when Ha_θ is small, which demonstrates that a certain strength of magnetic field is needed for instability.

2. The limit $\hat{k} \rightarrow \infty$

In the limit $\hat{k} \rightarrow \infty$, we have $\alpha \rightarrow 1$ so that the roots of (32) take the form [21, 30]

$$\begin{aligned} \frac{\lambda_{1,2}}{\Omega} &= N_A(2Rb - m^2) - im - \frac{1}{Re} \\ &\pm 2 \left\{ N_A^2(m^2 + Rb^2) + imN_A(2 + Ro) - 1 - Ro \right\}^{\frac{1}{2}}, \end{aligned} \quad (37)$$

where $N_A = Ha_\theta^2/Re$ is the Elsasser number for the azimuthal magnetic field [21, 30].

By expanding the eigenvalues (37) to first order in $1/Re$ we get [30, 46]

$$\begin{aligned} \frac{\lambda_{1,2}}{\Omega} &= -im \pm 2\sqrt{-(1 + Ro)} \\ &+ N_A \left(2Rb - m^2 \pm \frac{m(2 + Ro)}{\sqrt{1 + Ro}} \right) - \frac{1}{Re}. \end{aligned} \quad (38)$$

When $Ro < -1$, the instability occurs with the growth rate $\Re(\lambda)/\Omega \approx 2\sqrt{-(1 + Ro)}$. This mode pertains to the classical Rayleigh instability since no magnetic field is required.

When $Ro > -1$, the instability criterion becomes

$$\begin{aligned} -m^2 + |m| \frac{2 + Ro}{\sqrt{1 + Ro}} + 2Rb &> 0, \\ \text{and } Ha_\theta^2 &> \frac{\sqrt{1 + Ro}}{(2Rb - m^2)\sqrt{1 + Ro} + |m|(2 + Ro)}. \end{aligned} \quad (39)$$

If we choose that, e.g. $Rb = 0$ and $m = 1$, then $|Ha_\theta| \approx 0.8165$ is the onset of AMRI at the Keplerian $Ro = -3/4$ as shown in FIG. 3.

The left-hand side of the first of the inequalities (39) is a quadratic polynomial with respect to the real-valued number m . Hence, the discriminant of this polynomial

$$D = \frac{(2 + Ro)^2}{1 + Ro} + 8Rb > 0$$

in order that the polynomial can take positive values. This yields the familiar [29, 30] necessary condition for instability (29). For instance, for Keplerian flow $Ro = -3/4$ in (29) the inequality $Rb > -25/32$ is necessary for instability [29, 30].

The first inequality in (39) is written for Ro as

$$\begin{aligned} -1 < Ro < -2 + \frac{m^2 - 2Rb - \sqrt{(m^2 - 2Rb)^2 - 4m^2}}{2m^2(m^2 - 2Rb)^{-1}} \\ \text{or } Ro > -2 + \frac{m^2 - 2Rb + \sqrt{(m^2 - 2Rb)^2 - 4m^2}}{2m^2(m^2 - 2Rb)^{-1}}. \end{aligned} \quad (40)$$

When $m = \pm\sqrt{-2Rb}$ the domain (40) reduces to (30), which, at $Rb = -1$ takes the form

$$-1 < Ro < 2 - 2\sqrt{2} \quad \text{or} \quad Ro > 2 + 2\sqrt{2},$$

where $2 - 2\sqrt{2}$ and $2 + 2\sqrt{2}$ are the lower and the upper Liu limits, respectively [36].

3. Growth rate optimized by \hat{k} and \hat{q}

In the long wavelength limit of $\hat{k} \rightarrow 0$, $Rb < -1/4$ is necessary for the instability of $m = 1$ mode as shown by (36), while in the short wavelength limit of $\hat{k} \rightarrow \infty$, the condition $Rb > -\frac{1}{8} \frac{(Ro+2)^2}{Ro+1}$ given by (29) is necessary for the instability. Since the latter one overlaps with the former one, we conclude that for each value of Rb there exist wavenumbers \hat{k} and \hat{q} such that the mode with $m = 1$ is unstable.

Either the mode of $\hat{k} \rightarrow 0$ or $\hat{k} \rightarrow \infty$ dominate in large range of Rb , and the maximum growth rate is attained at a finite value of \hat{k} for every particular value of the magnetic Rossby number, Rb , as illustrated in FIG. 4. In this figure the optimized with respect to \hat{k} growth rate is plotted against Rb for $Re = 10^4$, $Ha_\theta = 100$, $m = 1$ and $Ro = -3/4$ and $\hat{q} = 0$ (upper panel) and $\hat{q} = 1$ (lower panel). We observe the crossover of the $\hat{k} = 0$ mode and the $\hat{k} = \infty$ mode. The range of large negative values of

Rb is dominated by the $\widehat{k} = 0$ mode and the one of large positive values of Rb is dominated by the $\widehat{k} \rightarrow \infty$ mode.

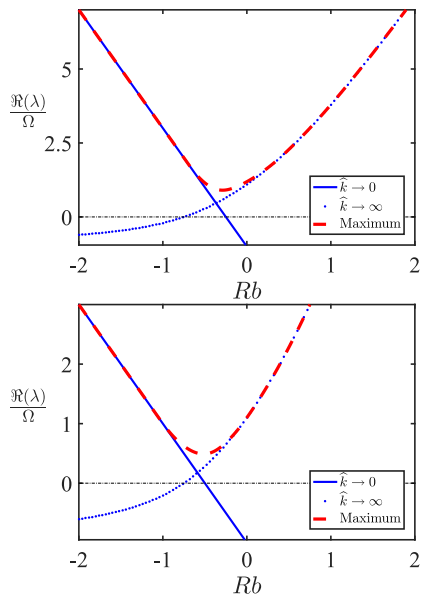


FIG. 4. The growth rate to magnetic Rossby number Rb for $Re = 10^4$, $Ha_\theta = 100$, $m = 1$, $Ro = -3/4$ and $\widehat{q} = 0$ (upper panel) or $\widehat{q} = 1$ (lower panel) according to (32). The solid line is $\widehat{k} = 0$ mode; the dotted one is the $\widehat{k} \rightarrow \infty$ mode and the dashed line stands for the growth rate maximized over \widehat{k} , whose left part tends to the $\widehat{k} = 0$ mode and the right part tends to the $\widehat{k} = \infty$, $\alpha = 1$ mode.

4. Evolution of AMRI region in the (Ro, Rb) -plane with \widehat{k}

In order to understand how the instability region evolves from that described by (36) at $\widehat{k} \rightarrow 0$ to (40) at $\widehat{k} \rightarrow \infty$ we plot the growth rate of the dispersion relation (31) in the projection to the (Rb, Ro) -plane, see FIG. 5. The results are presented over a growing set of axial wavenumber \widehat{k} for $Re = 10^4$, $Ha_\theta = 10^2$, $Pm = 10^{-6}$, $\widehat{q} = 1$, and $m = 1$. This choice of parameters is close to the inductionless approximation in strong magnetic fields.

It is clearly seen that already for $\widehat{k} > 1.9$ the neutral stability curve bounding the stability domain (shown in white in FIG. 5) is close to the inductionless one $Rb = -\frac{1}{8} \frac{(Ro+2)^2}{Ro+1}$. Equivalently, the instability domain is close to (40).

At the lower values of \widehat{k} the instability domain splits into two parts, one of which becomes dominant at $\widehat{k} = 1.2$ stretching along the Rb -axis at $\widehat{k} = 1$ and finally bifurcating into the instability domain corresponding to large negative values of Rb and practically not depending on Ro , in agreement with the criterion (36).

Below we demonstrate a similar transition for the domain of Taylor instability.

C. Taylor instability in the inductionless limit

Taylor [22, 45] established that an ideal nonrotating perfectly conducting fluid in an azimuthal magnetic field is stable against nonaxisymmetric perturbations with the azimuthal wavenumber $m = 1$ under the condition

$$\frac{d}{dr}(rB_\theta^2(r)) < 0. \quad (41)$$

Recalling the definition of the magnetic Rossby number (14) and taking into account that $B_\theta(r) = r\mu(r)$, the Taylor stability criterion for $m = 1$ takes the form:

$$Rb < -\frac{3}{4}, \quad (42)$$

which means that the azimuthal magnetic field $B_\theta(r) \sim r$ created by a current passing through a conducting fluid and corresponding to $Rb = 0$ is unstable.

The work [45] numerically predicted the Taylor instability (TI) caused by the field with $Rb = 0$ to exist also in the inductionless limit of $Pm \rightarrow 0$, which allowed for its recent observation in the experiments with liquid metals [47].

Using the geometrical optics stability analysis Kirillov et al. [30] extended the criterion for the onset of the inductionless Taylor instability to the case of arbitrary $m \geq 1$

$$Rb > \frac{m^2}{4\alpha^2} - 1, \quad (43)$$

where $\alpha = \widehat{k}^2 / (\widehat{k}^2 + \widehat{q}^2)$. When $m = \pm 1$ and $\alpha = 1$, which corresponds to the limit $\widehat{k} \rightarrow \infty$, the criterion (43) yields $Rb > -3/4$ for instability, which includes the case of $Rb = 0$ observed in the experiment [47].

In order to explore the Taylor instability on the base of the dispersion relation (31), we assume $Re = 0$ in it and take into account the relation

$$\frac{Re\sqrt{Pm}}{\Omega} = \frac{Ha_\theta}{\omega_{A\theta}}. \quad (44)$$

This reduces (31) to

$$\begin{aligned} & \left[\left(\frac{\lambda Ha_\theta}{\omega_{A\theta}} + \sqrt{Pm} \right) \left(\frac{\lambda Ha_\theta}{\omega_{A\theta}} + \frac{1}{\sqrt{Pm}} \right) + Ha_\theta^2 m^2 \right]^2 (\widehat{h}^2 + \widehat{q}^2) \\ & - 4Ha_\theta^4 \widehat{k}^2 m^2 - 4Ha_\theta^2 \left((\widehat{k}^2 - m^2) Rb + \frac{m^2 \widehat{k}^2}{\widehat{h}^2} \right) \\ & \times \left[\left(\frac{\lambda Ha_\theta}{\omega_{A\theta}} + \sqrt{Pm} \right) \left(\frac{\lambda Ha_\theta}{\omega_{A\theta}} + \frac{1}{\sqrt{Pm}} \right) + Ha_\theta^2 m^2 \right] = 0. \end{aligned} \quad (45)$$

We consider the inductionless limit where Pm is very small. Then the growth rate is of $O(\sqrt{Pm})$ and we can renormalize the eigenvalue as

$$\lambda = \lambda_0 \sqrt{Pm}. \quad (46)$$

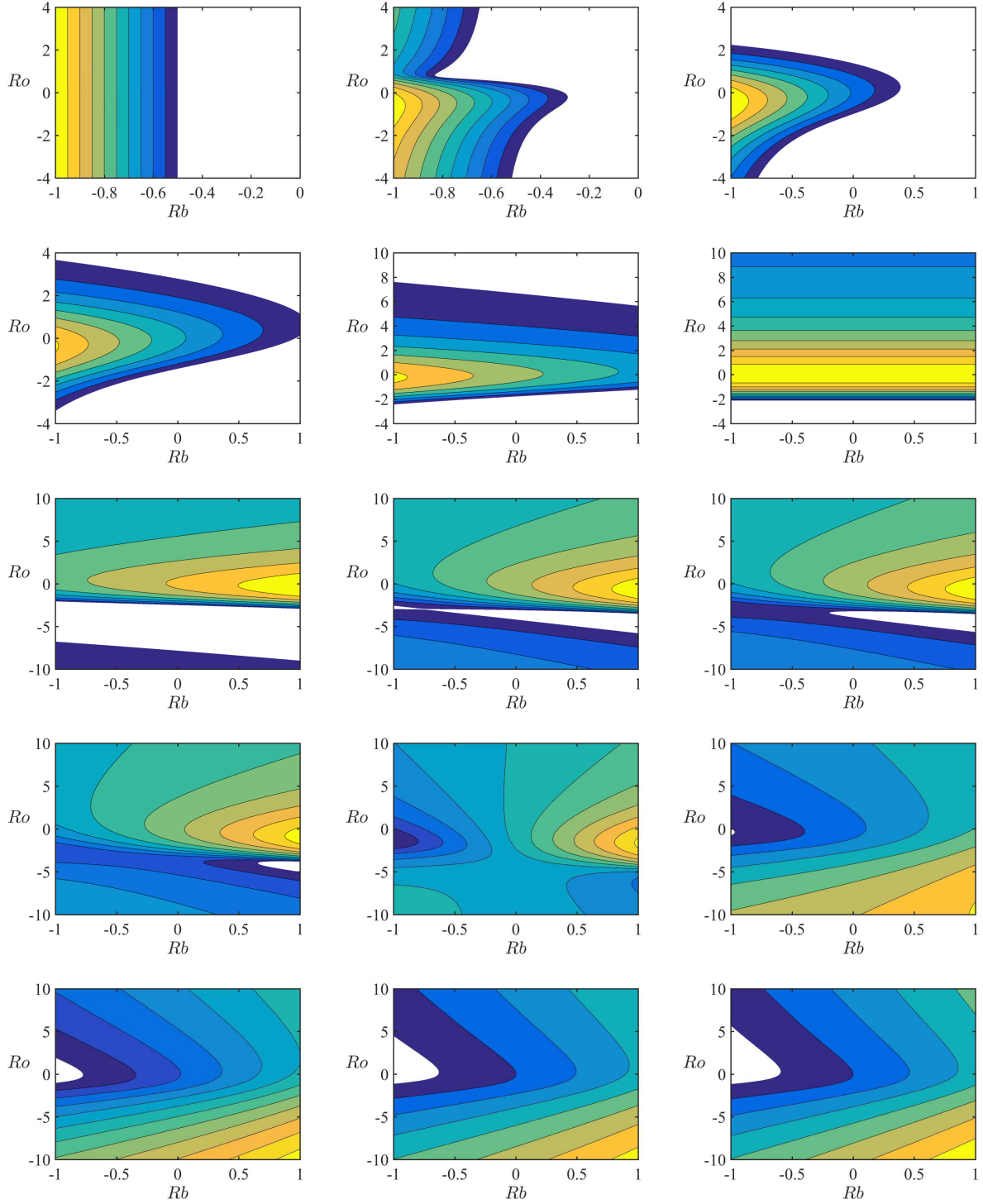


FIG. 5. Growth rate calculated with the use of the Hain-Lüst dispersion relation (32) in projection to the Rossby plane (Rb, Ro) for $Re = 10^4$, $Ha_\theta = 10^2$, $\hat{q} = 1$, $m = 1$ and (from upper-left to lower-right panel): $\hat{k} = 0.01, 0.4, 0.7, 0.8, 0.9, 1, 1.1, 1.17, 1.175, 1.2, 1.3, 1.8, 2.5, 5$ and 10 . The white domains represent stability.

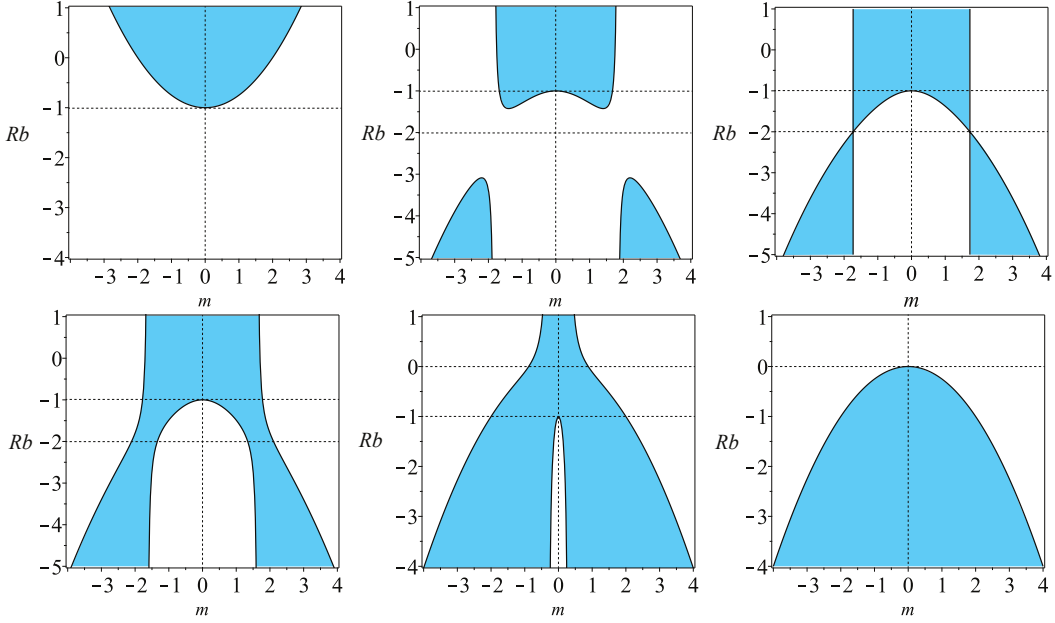


FIG. 6. The regions of the inductionless Taylor instability (blue) with the boundary (54) for $\hat{q} = 0$ and (top row from left to right) $\hat{k} = 100$, $\hat{k} = \sqrt{3} + 0.1$, and $\hat{k} = \sqrt{3}$ and (bottom row from left to right) $\hat{k} = \sqrt{3} - 0.1$, $\hat{k} = 0.3$, and $\hat{k} \rightarrow 0$.

Then the leading-order terms of (46) are

$$\begin{aligned} & \left(1 + \frac{\lambda_0}{\omega_{A\theta}} Ha_\theta + Ha_\theta^2 m^2\right)^2 (\hat{h}^2 + \hat{q}^2) \\ & - 4Ha_\theta^4 \hat{k}^2 m^2 - 4Ha_\theta^2 \left[(\hat{k}^2 - m^2) Rb + \frac{m^2 \hat{k}^2}{\hat{h}^2} \right] \\ & \times \left(1 + \frac{\lambda_0}{\omega_{A\theta}} Ha_\theta + Ha_\theta^2 m^2\right) = 0. \end{aligned} \quad (47)$$

For very large magnetic field we have $Ha_\theta \gg 1$, and can further renormalize the eigenvalue as

$$\lambda_0 = \lambda_a Ha_\theta. \quad (48)$$

and solve (47) for λ_a , to the leading order in Ha_θ^{-1} , as

$$\begin{aligned} \frac{\lambda_a}{\omega_{A\theta}} = & -m^2 + \frac{2}{\hat{h}^2 + \hat{q}^2} \left\{ (\hat{k}^2 - m^2) Rb + \frac{m^2 \hat{k}^2}{\hat{h}^2} \right. \\ & \left. \pm \sqrt{\left[(\hat{k}^2 - m^2) Rb + \frac{m^2 \hat{k}^2}{\hat{h}^2} \right]^2 + m^2 \hat{k}^2 (\hat{h}^2 + \hat{q}^2)} \right\}. \end{aligned} \quad (49)$$

In the limit of $\hat{k} \rightarrow 0$, equation (49) yields

$$\frac{\lambda_a}{\omega_{A\theta}} = \frac{\pm 2m^2 Rb - m^2 (\hat{q}^2 + m^2 + 2Rb)}{\hat{q}^2 + m^2}. \quad (50)$$

One of the roots (50) is equal to $-m^2$, whereas another one becomes positive if

$$Rb < -\frac{1}{4}(m^2 + \hat{q}^2) \quad (51)$$

reproducing the first of the inequalities (36).

In the limit of $\hat{k} \rightarrow \infty$, equation (49) reduces to

$$\begin{aligned} \frac{\lambda_a^\pm}{\omega_{A\theta}} &= 2Rb - m^2 \pm 2\sqrt{Rb^2 + m^2} \\ &= (1 + Rb)^2 - \left(1 \mp \sqrt{Rb^2 + m^2}\right)^2. \end{aligned} \quad (52)$$

The root $\lambda_a^-/\omega_{A\theta}$ in (52) is always negative. The other,

$$\frac{\lambda_a^+}{\omega_{A\theta}} = \left(Rb + \sqrt{Rb^2 + m^2}\right) \left(2 + Rb - \sqrt{Rb^2 + m^2}\right),$$

is a product of two expressions, the first of which is always positive whereas $2 + Rb - \sqrt{Rb^2 + m^2}$ is positive if

$$Rb > \frac{m^2}{4} - 1 \quad (53)$$

in accordance with (43), where $\alpha = 1$ because $\hat{k} \rightarrow \infty$. Therefore in the short axial wavelength approximation we reproduce the result [30]. Note that Ogilvie and Pringle [7] established criterion (53) for the case of ideal MHD.

In general, setting the right hand side of (49) to zero, we get the critical Rb at the neutral stability surface

$$Rb = \frac{1}{4} \left\{ \frac{\hat{q}^2 m^2}{\hat{k}^2 - m^2} + \frac{\hat{k}^2 (m^2 - 4)(\hat{k}^2 + 2m^2) + m^6}{\hat{k}^4 - m^4} \right\}. \quad (54)$$

For $\hat{k} = 0$ the expression (54) yields the critical value of the criterion (51) and for $\hat{k} \rightarrow \infty$ the critical value of the criterion (53).

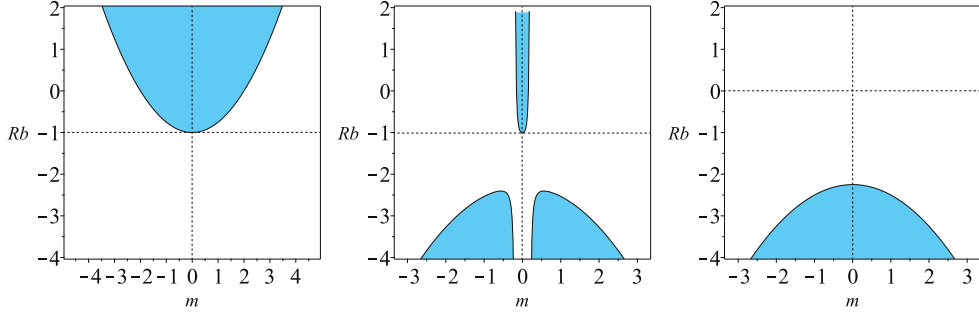


FIG. 7. The regions of the inductionless Taylor instability (blue) with the boundary (54) for $\hat{q} = 3$ and (from left to right) $\hat{k} = 100$, $\hat{k} = 0.2$, and $\hat{k} \rightarrow 0$.

FIG. 6 illustrates the transition from the criterion (53) to the criterion (51) as \hat{k} varies from 100 to 0 at the fixed $\hat{q} = 0$, based on the expression (54). At the value

$$\hat{k} = \sqrt{3 - \frac{1}{2}\hat{q}^2} \quad (55)$$

(equal to $\sqrt{3}$ for $\hat{q} = 0$ in FIG. 6) there are two saddle points at

$$Rb = \frac{1}{8}\hat{q}^2 - 2 \quad \text{and} \quad m = \pm\sqrt{3 - \frac{1}{2}\hat{q}^2}, \quad (56)$$

corresponding to $Rb = -2$ and $m = \pm\sqrt{3}$ in FIG. 6. The saddle points are formed by the straight lines $m = \pm\sqrt{3 - \frac{1}{2}\hat{q}^2}$ intersecting with the curve

$$Rb = \frac{2m^4 + (18 - \hat{q}^2)m^2 - 4\hat{q}^2 + 24}{4(\hat{q}^2 - 2m^2 - 6)}.$$

Note that (56) implies an upper bound on the value of \hat{q} : $|\hat{q}| < \sqrt{6}$. In these conditions the bifurcation value (55) for the parameter \hat{k} sharply separates the cases of the short-axial-wavelength (53) and long-axial-wavelength (51) inductionless Taylor instability. However, in the case $|\hat{q}| > \sqrt{6}$ the saddle point is absent and the transition scenario simplifies, see FIG. 7

VI. AMRI AND TAYLER INSTABILITY AT FINITE Pm

The magnetorotational instability is, by definition, caused by the cooperative effect of rotating flow field and magnetic field. The cooperative action comes into play for a differential rotation. Assuming the expansion of the solution in terms of Re as $\lambda^\pm/\omega_{A\theta} = a_0 Re + a_1 + a_2 Re^{-1} + a_3 Re^{-2} + \dots$, we expand the dispersion relation (31) with respect to $1/Re$ and solve the leading-order term to obtain a_0 . We repeat the process to find the coefficient a_1

from the next-order term resulting in the following representation for the critical roots at large Re :

$$\frac{\lambda^\pm}{\omega_{A\theta}} = -im \frac{Re\sqrt{Pm}}{Ha_\theta} - \frac{1}{Ha_\theta\sqrt{Pm}} \pm m \frac{\sqrt{-Ro(Ro+1)}}{Ro+1} + O\left(\frac{1}{Re}\right). \quad (57)$$

The growing wave $\Re(\lambda) > 0$ for the particular case of Keplerian flow ($Ro = -3/4$) with $m = 1$ is admitted for

$$Ha_\theta > \frac{1}{\sqrt{3Pm}}. \quad (58)$$

Since $Pm \sim 10^{-6}$ for the liquid metals used in the existing and planned experiments [12, 48, 49], the criterion (58) implies strong magnetic fields for the detection of AMRI.

In the PROMISE laboratory facility [12], the experimental setup is a Taylor-Couette flow between two co-rotating cylinders of finite axial size. The inner cylinder is set with the radius $r_{\text{in}} = 40\text{mm}$ and the outer cylinder is with $r_{\text{out}} = 2r_{\text{in}} = 80\text{mm}$. The gap between the cylinders is $d = r_{\text{out}} - r_{\text{in}} = r_{\text{in}}$. By that reason, in this section we assume $r_{\text{in}} = d = r_0$. Recalling (14), we can write

$$\Omega(r_{\text{in}}) = \Omega(r) \left(\frac{r_0}{r}\right)^{2Ro}, \quad \mu(r_{\text{in}}) = \mu(r) \left(\frac{r_0}{r}\right)^{2Rb}. \quad (59)$$

This allows us to redefine the Reynolds and Hartmann numbers as follows

$$Re_1 = \frac{\Omega(r_{\text{in}})d^2}{\nu} = Re|\mathbf{k}|^2 r_0^2 \left(\frac{r_0}{r}\right)^{2Ro},$$

$$Ha_{\theta_1} = \frac{\mu(r_{\text{in}})d^2}{\sqrt{\rho\mu_0\nu\eta}} = Ha_\theta|\mathbf{k}|^2 r_0^2 \left(\frac{r_0}{r}\right)^{2Rb}, \quad (60)$$

where $|\mathbf{k}|^2 = k^2 + q^2 + m^2/r^2$ and Re and Ha_θ are given by (16). The new Reynolds and Hartmann numbers (60) match those of the numerical and experimental works [12, 14, 39].

The critical Reynolds number at the onset of instability is crucial for the experimental realization of the MRI. The

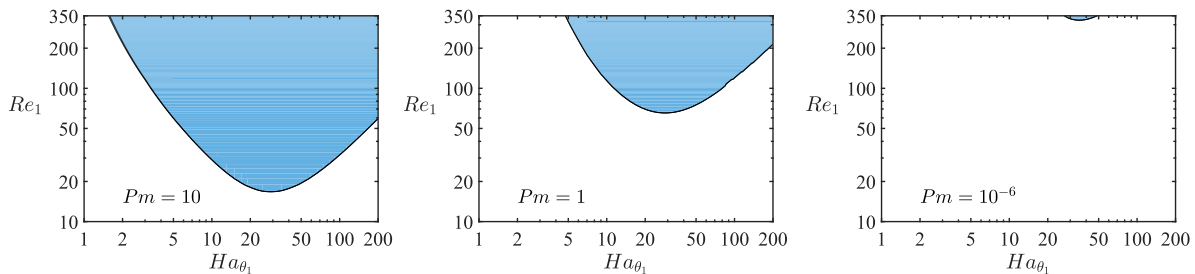


FIG. 8. AMRI regions (above the neutral stability curves) in the (Ha_{θ_1}, Re_1) -plane for $Rb = Ro = -1$, $m = 1$, $q = 3r_0^{-1}$, $r = 1.5r_0$ and (left to right) $Pm = 10$, $Pm = 1$, and $Pm = 10^{-6}$ found with the use of the growth rates maximized over k .

liquid metals used in the experiments have $Pm \sim 10^{-6}$, and the standard MRI which scales with the magnetic Reynolds number and the Lundquist number corresponds to the Reynolds numbers of order 10^6 . Therefore it is hard to maintain the basic flow undisturbed before the onset of SMRI [50, 51].

The helical and the azimuthal MRI scale with the Reynolds and Hartmann numbers and thus require moderate ranges of the Reynolds numbers compared to SMRI [9]. By that reason both HMRI and AMRI were detected in the laboratory experiments [12, 48, 49, 52, 53] for rotation which is a little bit shallower than the Rayleigh value $\Omega \sim r^{-1.9}$ and for the current-free azimuthal magnetic field corresponding to $Rb = -1$. In [21, 29] it was theoretically shown that the inductionless HMRI and AMRI for the Keplerian flow with $Ro = -3/4$ exist when the radial dependence of the azimuthal magnetic field is shallower than that of the current-free type: $Rb > -\frac{1}{8} \frac{(Ro+2)^2}{Ro+1}$. In section V, we have verified this result for large axial wavenumbers, $k \gg 1$. The planned AMRI-TI experiment in the frame of the new DRESDYN facility [48, 49] creates the azimuthal magnetic field both due to currents isolated of the liquid metal and passing directly through the metal thus allowing for variable Rb including those satisfying the instability criterion (29).

On the other hand, in section V we have found that for small axial wavenumbers, $k \ll 1$, the inductionless AMRI of the Keplerian flow may occur at $Rb < -1/4$, which includes the current-free azimuthal magnetic field with $Rb = -1$ used in the existing PROMISE experiment, see FIG. 4. Using the redefined Reynolds and Hartmann numbers (60) in this section we compare our WKB-analysis with the results from the global analysis [13, 39] for arbitrary Pm and discuss the implications for the experimental detection of the long-axial-wavelength instability. In view of the recent discovery of a long-wavelength linear instability of a hydrodynamical Taylor-Couette flow [42] this direction is worth pursuing.

A. Case of $Ro = Rb = -1$ and $m = 1$ with $q = 3r_0^{-1}$

Since the Taylor-Couette experimental apparatus is radially bounded, we limit q from below and choose e.g. $q = 3r_0^{-1}$, which is reasonable when the radial velocity disturbance should be zero on the boundary and the width between the two cylinders is r_0 . In FIG. 8 we present the instability region in the (Ha_{θ_1}, Re_1) -plane. To find it, we numerically calculate the maximum growth rate at every meshing point in the (Ha_{θ_1}, Re_1) -plane for a wide range of k . Zero growth rates correspond to the neutral stability curve. The calculation is performed locally at $r = 1.5r_0$, the average of $r_{in} = r_0$ and $r_{out} = 2r_0$. Notice that the Taylor instability is excluded in this parameter regime by (51) and (53). We can see that FIG. 8 is similar to Figure 1 of Hollerbach et al. [13] and Figure 1 of Rüdiger et al. [14]. The instability is invited when the Reynolds number is of the order 10^2 when $Pm \ll 1$ and of the order 10 when $Pm \approx 1, 10$. When $Pm = 10^{-6}$, the critical Reynolds number is $Re_1 \approx 324$ which is attained at $Ha_{\theta_1} \approx 34$, $k = 2.6777r_0^{-1}$ and $q = 3r_0^{-1}$.

The left panel of FIG. 9 shows that for $Re_1 = 3000$ and $Pm = 10^{-6}$, the instability occurs when $Ha_{\theta_1} \in (15, 583)$. The growth rate has its extremum $\Re(\lambda_{max})/\Omega_{in} \approx 0.1385$ at $Ha_{\theta_1} \approx 162$ with the extremizer $k \approx 5.5r_0^{-1}$. On the right panel of FIG. 9 corresponding to $Re_1 = 500$, the instability occurs for $Ha_{\theta_1} \in (20, 85)$. The growth rate reaches its extremum $\Re(\lambda_{max})/\Omega_{in} \approx 0.0438$ at $Ha_{\theta_1} \approx 47$ with the extremizer $k \approx 3.159r_0^{-1}$. We see that in both cases no instability occurs when the magnetic field is sufficiently weak in agreement with the argument in Section V A.

B. Case of $Ro = Rb = -1/2$ and $m = 1$ with $q = 3r_0^{-1}$

The magnetic Rossby number $Rb = -1/2$ and the azimuthal wavenumber $m = 1$ lie inside the range (53) and thus allow for the emergence of Taylor instability [22, 39]. FIG. 10 displays the variation of the instability regions in (Ha_{θ_1}, Re_1) plane when the magnetic Prandtl number Pm changes from 100 to 0.1. This result compare well with Figure 3 of Rüdiger et al. [39]. We notice that

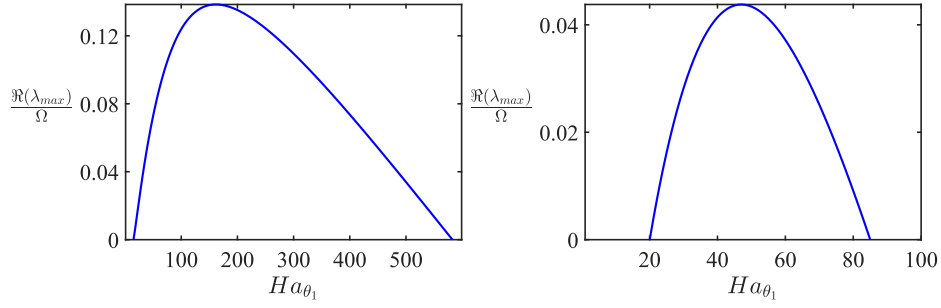


FIG. 9. The maximized over k growth rate $\Re(\lambda_{max})$ in the units of Ω versus Ha_{θ_1} for the flow with $Ro = -1$, $Rb = -1$, $Pm = 10^{-6}$, $m = 1$, $q = 3r_0^{-1}$, and $r = 1.5r_0$ when (left) $Re_1 = 3000$ and (right) $Re_1 = 500$.

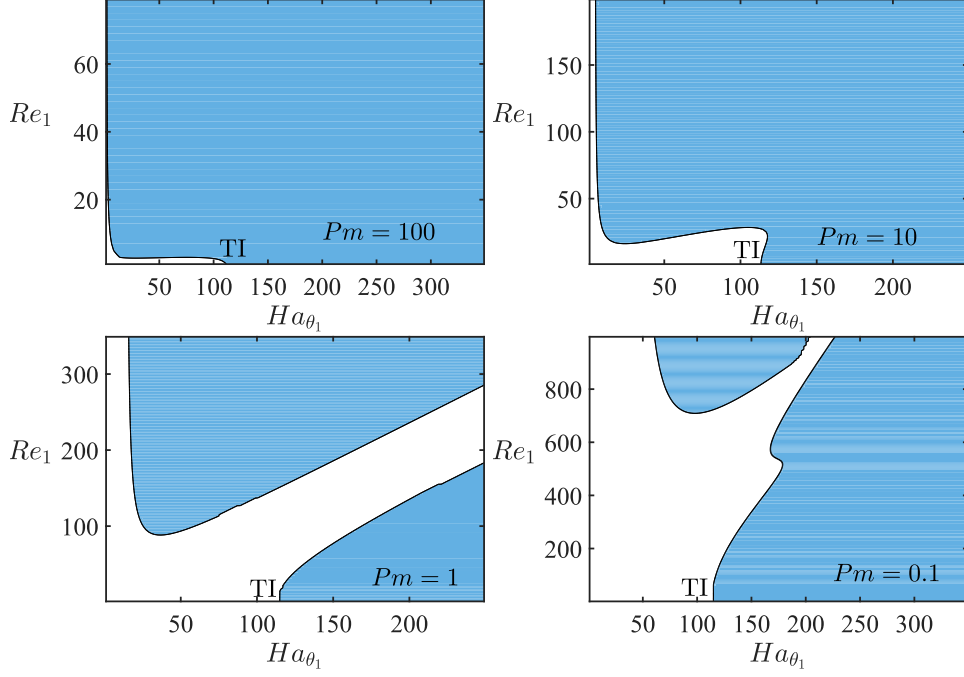


FIG. 10. The instability region in the (Re_1, Ha_{θ_1}) -plane for $Ro = -1/2$, $Rb = -1/2$, $m = 1$, $q = 3r_0^{-1}$, $r = 1.5r_0$, and $Pm = 100$, $Pm = 10$, $Pm = 1$, and $Pm = 0.1$. The instability domains represented in blue are found with the use of the growth rates maximized over k .

there are two types of instabilities, with the lower part originating from the Taylor instability occurring without rotation in the basic state, and with the upper part originating from the AMRI. As Pm decreases, the critical Reynolds number becomes larger for the AMRI and the AMRI region shrinks to a seemingly separate upper region. The critical Hartmann number for the Taylor instability turns out to be insensitive to Pm . FIG. 10 exhibits marked contrast with FIG. 8 where TI is excluded by the criteria (51) and (53).

Closer to the experimental condition is the case of $Pm = 0.1$ in FIG. 10. Fixing $Pm = 0.1$ and $Re_1 = 800$, we draw the optimized over k growth rate as a function of Ha_{θ_1} in FIG. 11. There are two instability intervals $Ha_{\theta_1} \in (71, 153) \cup (195, \infty)$. In the first one a local ex-

tremum is attained at $Ha_{\theta_1} \approx 112$ with the wavenumbers $k = 1.8352r_0^{-1}$ and $q = 3r_0^{-1}$. The growth rate increases monotonically with Ha_{θ_1} for $Ha_{\theta_1} > 195$.

C. Case of $Ro = -3/4$, $Rb = -1$ and $m = 1$ with $q = 3r_0^{-1}$

According to the instability condition (29) the Keplerian rotation with $Ro = -3/4$ cannot be destabilized by the current-free azimuthal magnetic field with $Rb = -1$ in the inductionless limit of $Pm = 0$. Instead, the criterion (29) suggests shallower radial profiles for the magnetic field with $Rb > -25/32$. Does this change for small but finite Pm ? The work [30] predicted regions of HMRI

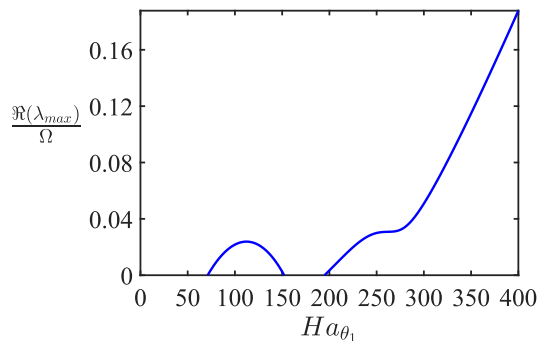


FIG. 11. The optimized over k growth rate versus the Hartmann number Ha_{θ_1} . The parameters chosen are $Re_1 = 800$, $Rb = -1/2$, $Ro = -1/2$, and $Pm = 0.1$ with $m = 1$, $q = 3r_0^{-1}$, and $r = 1.5r_0$.

existing at such values of the magnetic Prandtl number. What can we say about AMRI?

Here we demonstrate that, for $Ro = -3/4$ and $Rb = -1$, there is a minimum value of the magnetic Prandtl number Pm , below which the instability is ruled out. Let us choose $r = 1.5r_0$ and search for the critical Pm for instability. For the flow with $Re_1 = 10^4$, the left panel of FIG. 12 shows that the instability necessitates $Pm > 0.0046$, with the critical value of Pm corresponding to $Ha_{\theta_1} \approx 400$. For $Re_1 = 10^3$, the critical value is raised to $Pm \approx 0.048$ which is attained at $Ha_{\theta_1} \approx 127$ as shown by the right panel of FIG. 12.

As Re_1 is increased, the critical value of Pm is decreased, which yields a larger strength of magnetic field according to (58). Large Reynolds numbers mean turbulence in practice so that $Pm \gtrsim 10^{-3}$ is at least necessary for experimental realization of the AMRI. However the liquid eutectic alloy $Ga^{67}In^{20.5}Sn^{12.5}$ has $Pm = 1.4 \times 10^{-6}$ making the AMRI of a Keplerian flow virtually impossible for the experimental setup with the current-free azimuthal magnetic field [12]. Indeed, FIG. 13 shows that as Pm decreases, the instability region becomes smaller and smaller.

However, as FIG. 4 demonstrates, in the inductionless limit ($Pm \rightarrow 0$), the $k \rightarrow 0$ mode has positive growth rate. To approach this instability, we set $r_{out} = r_0$ as the characteristic length but set r to vary freely toward $r = 0$. By setting $\hat{k} = 0$ in (32), we find its roots in the following form

$$\begin{aligned} \frac{\lambda_1}{\Omega} &= -\sqrt{\frac{r_0}{r}} \frac{1}{1+(qr)^2} \frac{Ha_{\theta_1}^2}{Re_1} - \sqrt{\frac{r_0}{r}} \frac{1+(qr)^2}{Re_1} - i, \\ \frac{\lambda_2}{\Omega} &= \sqrt{\frac{r_0}{r}} \frac{3-(qr)^2}{(1+(qr)^2)^2} \frac{Ha_{\theta_1}^2}{Re_1} - \sqrt{\frac{r_0}{r}} \frac{1+(qr)^2}{Re_1} \\ &\quad + i \frac{2-(qr)^2}{1+(qr)^2}. \end{aligned} \quad (61)$$

The first root has $\Re(\lambda_1) < 0$ and corresponds to a stable mode. The second one indicates that, for large

values of Ha_{θ_1} , the instability occurs when

$$(qr)^2 < 3. \quad (62)$$

In addition, the radial wavenumber is bounded so as to satisfy the boundary conditions at the cylinders of $r = r_{in}$ and r_{out} , indicating

$$q(r_{out} - r_{in}) > \pi > 3. \quad (63)$$

Combining (62) and (63), we obtain

$$\frac{r}{r_{out} - r_{in}} < \frac{1}{\sqrt{3}} \quad (64)$$

Because $r > r_{in}$, $r_{in}/(r_{out} - r_{in}) < 1/\sqrt{3}$, namely

$$\frac{r_{in}}{r_{out}} < \frac{\sqrt{3}-1}{2} \approx 0.366. \quad (65)$$

This crude argument suggests that the experimental setups with $r_{in}/r_{out} = 1/2$ might need to be modified to have a wider gap in order to be able to capture the mode of $k = 0$ for a Keplerian flow subject to the current-free magnetic field.

VII. GLOBAL STABILITY ANALYSIS

In order to provide a numerical validation of the analytical results based on the Hain-Lüst dispersion relation (31), in the following we consider the cylindrical Taylor-Couette flow as described in Section VI. We will decompose the magnetic and velocity fields into toroidal and poloidal parts and after that reduce the original MHD system (3)–(6) to a one-dimensional boundary eigenvalue problem [37, 54] by expanding the solution in the Heinrichs basis [41, 44, 55].

We assume a finite radial gap $d := |r_{out} - r_{in}|$ and a radius ratio $\zeta := r_{in}/r_{out}$ that both define the geometry of the setup. Our numerical method is based on the pseudo-spectral expansion of the solution in terms of normal modes before collocating at the Chebyshev-Gauss nodes. The code we have developed has been benchmarked against several well-established results of similar stability analysis for either insulating or conducting boundary conditions with excellent agreement.

For the sake of clarity, we first render the problem (3)–(6) in a dimensionless form following the notations in Child et al. [37] except for the background velocity field where we follow the work of Deguchi [44]. This can be summarized by scaling length with d , time with the viscous time scale d^2/ν , velocities with ν/d , pressure with $\rho\nu^2/d^2$ and magnetic fields with B_0 .

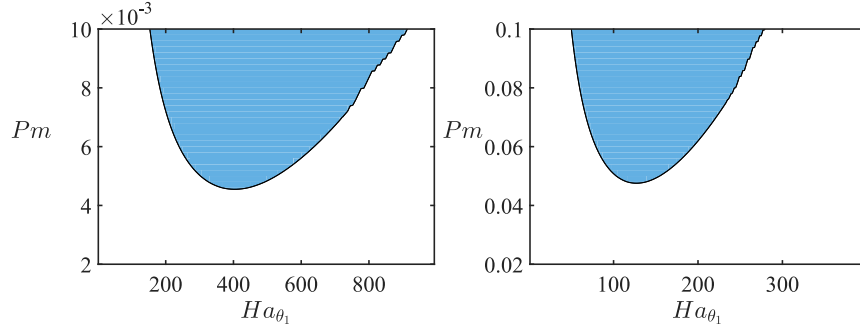


FIG. 12. The region of AMRI (above the critical lines) in the (Ha_{θ_1}, Pm) -plane when $Rb = -1$, $Ro = -3/4$ and (left) $Re_1 = 10^4$ and (right) $Re_1 = 10^3$. In the former case the instability occurs when $Pm > 0.0046$ with the smallest Pm corresponding to $Ha_{\theta_1} \approx 400$ whereas in the latter when $Pm > 0.048$ with the lowest Pm corresponding to $Ha_{\theta_1} \approx 127$.

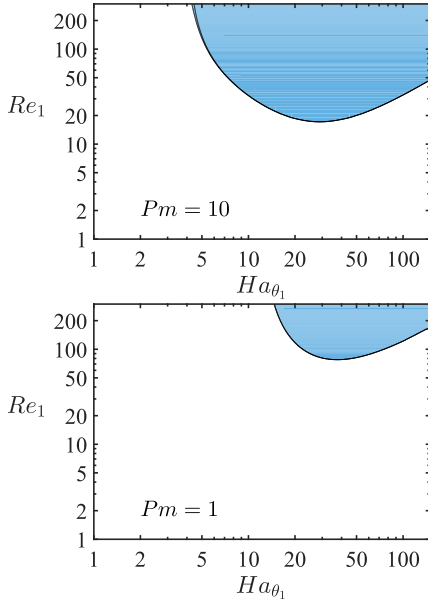


FIG. 13. The region of AMRI in the (Ha_{θ_1}, Re_1) -plane when $Ro = -3/4$ and $Rb = -1$, $m = 1$, $q = 3r_0^{-1}$ and $r = 1.5r_0$. The neutral stability curve is obtained by maximizing the growth rate over k for $Pm = 10$ and $Pm = 1$.

A. Background fields and Rossby numbers

The scaling introduced before leads to the following set of equations

$$\begin{aligned}
 \frac{\partial \hat{\mathbf{u}}}{\partial t} &= -(\hat{\mathbf{u}} \cdot \hat{\nabla}) \hat{\mathbf{U}} - (\hat{\mathbf{U}} \cdot \hat{\nabla}) \hat{\mathbf{u}} - \hat{\nabla} \hat{P} + \hat{\nabla}^2 \hat{\mathbf{u}} \\
 &\quad + \frac{Ha_{\theta}^2}{Pm} \left[(\hat{\mathbf{b}} \cdot \hat{\nabla}) \hat{\mathbf{B}} + (\hat{\mathbf{B}} \cdot \hat{\nabla}) \hat{\mathbf{b}} \right], \\
 \frac{\partial \hat{\mathbf{b}}}{\partial t} &= \hat{\nabla} \times (\hat{\mathbf{U}} \times \hat{\mathbf{b}}) + \hat{\nabla} \times (\hat{\mathbf{u}} \times \hat{\mathbf{B}}) + \frac{1}{Pm} \hat{\nabla}^2 \hat{\mathbf{b}}, \\
 \hat{\nabla} \cdot \hat{\mathbf{u}} &= 0, \\
 \hat{\nabla} \cdot \hat{\mathbf{b}} &= 0,
 \end{aligned} \tag{66}$$

where $Ha_{\theta} = B_0 d / \sqrt{\rho \mu_0 \nu \eta}$ is the azimuthal Hartmann number and $Pm = \nu / \eta$ is the magnetic Prandtl number.

This dimensionless MHD system is therefore solved regarding to no-slip boundary conditions for the velocity field, which in the cylindrical coordinates (r, θ, z) lead to [42]

$$\begin{aligned}
 \hat{U}_{\theta}(r_{in}, \theta, z) &= \frac{\Omega_{in} r_{in} d}{\nu} =: Re_{in}, \\
 \hat{U}_{\theta}(r_{out}, \theta, z) &= \kappa Re_{in} / \zeta =: Re_{out},
 \end{aligned} \tag{67}$$

where \hat{U}_{θ} is the azimuthal component of the fluid velocity, $\kappa := \Omega_{out} / \Omega_{in}$ is the ratio between the angular velocities and the inner and outer radii can be defined according to the Taylor-Couette parameters as $r_{in} := d\zeta / (1 - \zeta)$ and $r_{out} := d / (1 - \zeta)$.

A fundamental solution for this system and the boundary conditions is the well-known Couette profile $\hat{\mathbf{U}} = \hat{r} \Omega(\hat{r}) \mathbf{e}_{\theta}$, given by

$$\Omega(\hat{r}) = \frac{Re_{in}}{1 + \zeta} \left[\left(\frac{\kappa}{\zeta} - \zeta \right) + \frac{\zeta(1 - \kappa)}{(1 - \zeta)^2} \frac{1}{\hat{r}^2} \right], \tag{68}$$

where $\hat{r} = rd^{-1}$ is the dimensionless radial coordinate.

The background magnetic field we consider here is purely azimuthal $\hat{\mathbf{B}} = \hat{B}_{\phi}(\hat{r}) \mathbf{e}_{\theta}$ and given by

$$\hat{B}_{\phi}(\hat{r}) = \frac{\zeta(\tau - \zeta)}{1 - \zeta^2} \hat{r} + \frac{1 - \tau\zeta}{1 - \zeta^2} \frac{1}{\hat{r}}, \tag{69}$$

where $\tau := B_{out} / B_{in}$ is the ratio between the outer and the inner azimuthal magnetic fields [56].

Using (59) and (69) we can write

$$\begin{aligned}
 \kappa &= \zeta^{-2Ro}, \\
 \tau &= \zeta^{-(2Rb+1)}.
 \end{aligned} \tag{70}$$

Then, the solid-body rotation ($Ro = 0$) corresponds to $\kappa = 1$ and the Keplerian flow ($Ro = -3/4$) to $\kappa = \zeta^{3/2}$.

In the following, we will specify the basic state of the magnetized flow via Ro , Rb , ζ , Re_{in} , Pm and Ha_{θ} defined earlier.

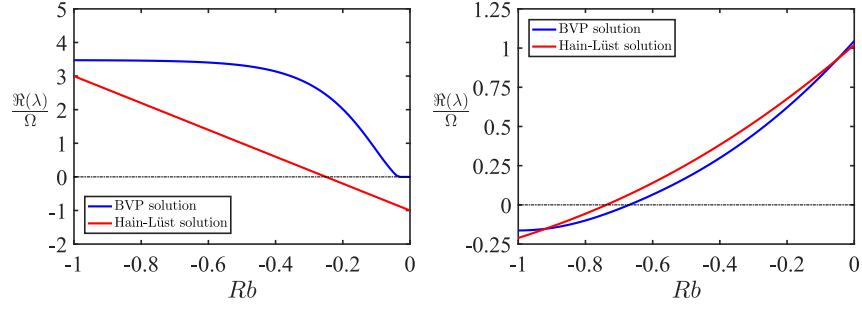


FIG. 14. The growth rate $\Re(\lambda)$ in units of Ω_{in} over a range of magnetic Rossby number Rb for the Keplerian ($Ro = -3/4$) flow with $Re_{in} = 10^4$, $Ha_\theta = 10^2$, $Pm = 0$, and $m = 1$, in the case of the long axial wavelength ($\zeta = 0.02$ and $k = 10^{-4}d^{-1}$, left panel) and short axial wavelength ($\zeta = 0.98$ and $k = 3.5d^{-1}$, right panel). The blue line comes from the dimensionless Taylor-Couette boundary value problem. The boundary conditions correspond to the perfectly conducting walls. The red lines correspond to the Hain-Lüst dispersion relation (32) and the radial wavenumber $\hat{q} = \zeta/(1 - \zeta)$, cf. FIG. 4.

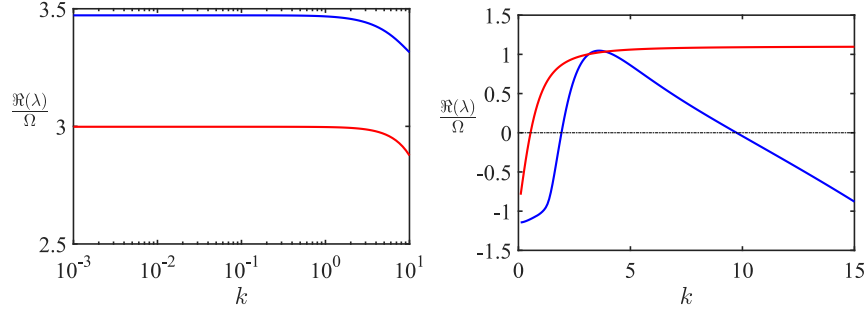


FIG. 15. The growth rate $\Re(\lambda)$ in the units of Ω_{in} from BVP (blue) and Hain-Lüst (red) optimized over the axial wavenumber k (in units of d^{-1}) for perfectly conducting boundaries with $\zeta = 0.02$, $Rb = -1$ (left) and $\zeta = 0.98$, $Rb = 0$ (right). The parameter space is the same as in FIG. 14.

B. Pseudo-spectral expansion

We seek for a solution to linearized MHD equations decomposed into toroidal and poloidal parts as follows

$$\tilde{\mathbf{u}} = \nabla \times (\psi \mathbf{e}_r) + \nabla \times \nabla \times (\phi \mathbf{e}_r), \quad (71)$$

$$\tilde{\mathbf{b}} = \nabla \times (\Psi \mathbf{e}_r) + \nabla \times \nabla \times (\Phi \mathbf{e}_r). \quad (72)$$

The disturbance fields (ψ, ϕ, Ψ, Φ) in (71)-(72) are expanded in terms of normal modes according to the pseudo-spectral Fourier method. In it, each variable is expressed with respect to Heinrichs basis [41, 44, 55] for the radial direction and to Fourier basis for the axial and azimuthal directions. Such expansion can be represented for an arbitrary field \mathcal{L} as

$$\mathcal{L}(x, t, \theta, z) := \sum_{n=0}^{\infty} [\mathcal{H}(x)T_n(x)] \exp[\lambda t + i(m\theta + kz)], \quad (73)$$

where $T_n(x)$ is a Chebyshev polynomial, $\mathcal{H}(x)$ is the Heinrichs factor which depends on the boundary conditions considered, λ is an eigenvalue, (m, k) are the azimuthal and axial wavenumbers and x is the length coordinate.

In order for the method to be computable, the infinite series are truncated at the N -th order and the map-

ping of the radial interval $[r_{in}, r_{out}]$ to the Chebyshev interval $[-1, 1]$ comes from the linear transformation [41] $x = 2(r - r_m)d^{-1}$ with $r_m = d(1 + \zeta)/(2(1 - \zeta))$ being the mean radius. Finally, the series are evaluated at the Chebyshev-Gauss collocation points

$$x_i = \pm \cos\left(\pi \frac{i+1}{N+2}\right), \quad i = 0, \dots, N.$$

The decomposition (73) allows us to express the differential operators as functions of the wavenumbers and parameters of the system. Details of this method and coefficients of the boundary value problem can be found, e.g., in Child et al. [37] and Hollerbach et al. [54]. The set of equations we obtain is solved regarding the boundary conditions considered, i.e., no-slip conditions for the velocity field and perfectly conducting for the magnetic field. Assuming the expansion in terms of normal modes for each variables, these conditions can be written in the following form [57]

$$\psi = \phi = \partial_r \phi = 0, \quad (74)$$

$$\Phi = 0, \quad (75)$$

$$ik\partial_r\Psi + ikr^{-1}\Psi + imr^{-1}\partial_{rr}\Phi - imr^{-2}\partial_r\Phi = 0. \quad (76)$$

The system is therefore reduced to a generalised eigenvalue problem of the form $A\xi = \lambda B\xi$, where λ is an

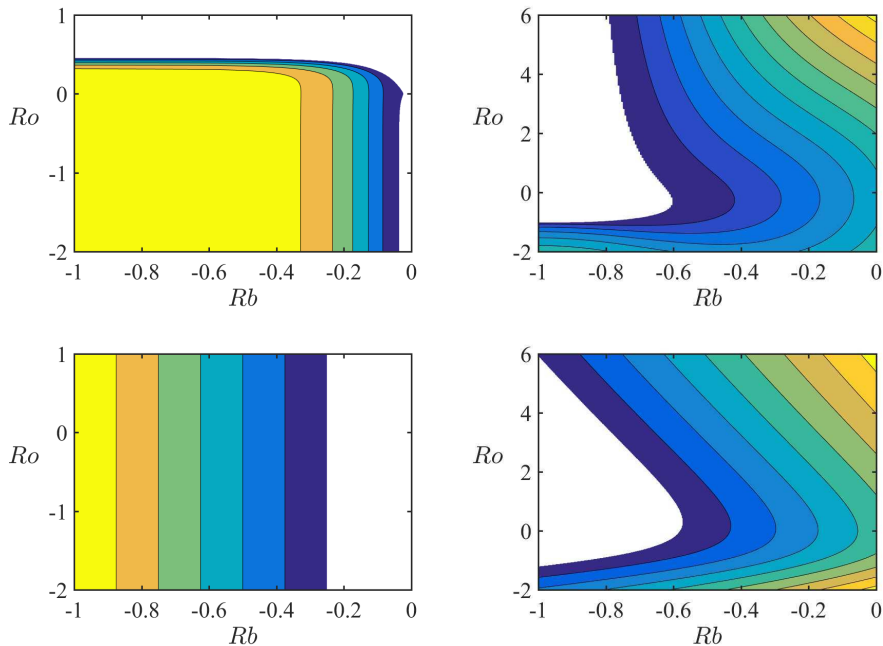


FIG. 16. Growth rate magnitude in the Rossby plane (Rb, Ro) from the boundary value problem with perfectly conducting boundaries for the upper panels and from Hain-Lüst dispersion relation (31) for the lower panels with $\zeta = 0.02$, $k = 10^{-4}d^{-1}$ (left column) and $\zeta = 0.98$, $k = 3.5d^{-1}$ (right column). Both figures are computed with $Re_{in} = 10^4$, $Ha_{\theta} = 10^2$ and $Pm = 0$ (BVP, left) or $Pm = 10^{-6}$ (BVP, right). Stability is represented in white.

eigenvalue and ξ an eigenvector.

C. Numerical results

For a fixed set of boundary conditions, the boundary value problem is solved and leads to the computation of the eigenvalues λ of the magnetized Taylor-Couette flow. The global stability analysis is therefore conducted over similar sets of parameters from the previous sections of this paper in order to validate a large part of the results.

In FIG. 14 we compare growth rates given by the boundary value problem and by the Hain-Lüst dispersion relation (31). The eigenvalues are both scaled with the inner angular velocity Ω_{in} . To reach the $k \rightarrow 0$ mode, we fix a wide radial gap in order to have a small radial wavenumber. We choose an arbitrary value for the gap between both cylinders $\zeta = 0.02$ and according to this geometry, we manage to find a similar behavior for the growth rate of the long-wavelength domain but with nevertheless a discrepancy for the threshold of instability. For the short-wavelength domain, we use a narrow-gap $\zeta = 0.98$ and the growth rates from the BVP and the Hain-Lüst dispersion relation are thus in good agreement.

The stability analysis has been conducted for different but finite radial gaps over different values of Rb in FIG. 14. The dependence of the growth rate on the axial wavenumber k in our numerical scheme is represented in FIG. 15 where we observe that for the long-wavelength

domain the growth rate reaches its maximum for $k \rightarrow 0$ as expected, cf. FIG. 1. For the short-wavelength domain, we are limited to a smaller interval of k for which the growth rate is positive for the boundary value problem but it is enough to produce correct computations. In that way, we are able to produce smooth results for both domains and recover established analytical results.

The last computation presents the stability domains in the (Rb, Ro) -plane as in the previous section VB 4. This case is presented in FIG. 16 where the growth rate magnitude from the BVP and from the dispersion relation (31) is computed in the (Rb, Ro) -plane with different set of parameters. The left column shows the long-wavelength instability domains with $\zeta = 0.02$ and $k = 10^{-4}d^{-1}$, and by comparing both figures we notice that the shape of the numerical domain is close to the theory.

For the short-wavelength computation, we have considered the Taylor-Couette flow with the same parameter space as for the long-wavelength case except for the gap and wavenumbers for which we choose $\zeta = 0.98$ and $k = 3.5d^{-1}$, see the right panels of FIG. 16 demonstrating a good agreement with the theory.

VIII. CONCLUSION

We have explored the AMRI and the Taylor instability of a rotating MHD flow, augmented by viscosity and electrical resistivity, with respect to the axisymmetric as well

as non-axisymmetric perturbations. We have derived the extended Hain-Lüst equation to include the viscosity and electrical resistivity. This is a second-order ordinary differential equation for the radial Lagrangian displacement.

We then applied the WKB approximation to it to derive a dispersion relation, valid in the regime of short wavelengths in the radial direction but allowing for arbitrary azimuthal and axial wavenumbers.

By that reason, the extended Hain-Lüst dispersion relation contains the previously known dispersion relations derived by different methods, including the geometrical optics approximation.

On the other hand, the additional terms in it enable more accurate treatment of the non-axisymmetric perturbations with large axial wavelength.

While being in the limit of short axial wavelength we restored the well-known results of the inductionless approximation, including the necessary condition (29) for both HMRI and AMRI, and the generalized Tayler instability condition (53), in the limit of long axial wavelength we discovered new instability that works both in the rotating and in the non-moving fluid.

We found a limitation on the radial wavelength providing an estimate for the gap in a Taylor-Couette setup which is necessary for detection of the new instability. Finally, we combined the numerical methods of Deguchi and Nagata [41, 42] and Child et al. [37] to validate the analytical findings, based on the Hain-Lüst dispersion relation, using global stability analysis.

ACKNOWLEDGMENTS

R.Z. was supported by a Ph.D. Studentship from the China Scholarship Council. J.L. was supported by a Ph.D. Scholarship from Northumbria University. Y.F. was supported in part by a Grant-in-Aid for Scientific Research from the Japan Society for the Promotion of Science (Grant No. 19K03672).

Appendix A: Derivation of equation (11)

In this appendix we derive the extended Hain-Lüst equation (11). The lines 4–6 in (8) allow us to express the magnetic field disturbance \tilde{b}_r , \tilde{b}_θ , and \tilde{b}_z in terms of the other variables. By eliminating the magnetic field disturbances, we can reduce (8) to equations for $\boldsymbol{\xi}_1 = (\tilde{u}_r, \tilde{u}_\theta, \tilde{u}_z, \tilde{p})$ as

$$\mathbf{M}_1 \boldsymbol{\xi}_1 = 0, \quad (\text{A1})$$

where, with use of (9)

$$\mathbf{M}_1 = \begin{pmatrix} \Lambda + \frac{2\mu r}{\rho\mu_0\tilde{\lambda}_\eta} \left(\frac{iF}{\tilde{\lambda}_\eta} \Omega' - \mu' \right) & -2\Omega + \frac{2iF\mu}{\rho\mu_0\tilde{\lambda}_\eta} & 0 & \frac{1}{\rho} \frac{d}{dr} \\ 2\Omega + r\Omega' \left(1 + \frac{F^2}{\rho\mu_0\tilde{\lambda}_\eta^2} \right) - \frac{2iF\mu}{\rho\mu_0\tilde{\lambda}_\eta} & \Lambda & 0 & \frac{1}{r\rho} im \\ 0 & 0 & \Lambda & \frac{1}{\rho} ik \\ \frac{1}{r} + \frac{d}{dr} & \frac{im}{r} & ik & 0 \end{pmatrix} \quad (\text{A2})$$

and the prime denotes the derivative with respect to r .

We then combine all the equations into a single second-order differential equation for the radial component of the Lagrangian displacement field. As an intermediate step, we solve algebraic equations (A1) and express $(\tilde{u}_r, \tilde{u}_\theta, \tilde{u}_z)$ in terms of \tilde{p} as

$$\begin{aligned} \tilde{u}_r &= -\frac{\Lambda}{E\rho} \frac{d\tilde{p}}{dr} + \frac{im}{E\rho r} \left(\frac{2iF\mu}{\tilde{\lambda}_\eta\rho\mu_0} - 2\Omega \right) \tilde{p}, \\ \tilde{u}_\theta &= \frac{1}{E\rho} \left[2\Omega + r\Omega' \left(1 + \frac{F^2}{\rho\mu_0\tilde{\lambda}_\eta^2} \right) - \frac{2iF\mu}{\rho\mu_0\tilde{\lambda}_\eta} \right] \frac{d\tilde{p}}{dr} \\ &\quad - \frac{im}{Er\rho} \left[\Lambda + \frac{2\mu r}{\rho\mu_0\tilde{\lambda}_\eta} \left(\frac{iF}{\tilde{\lambda}_\eta} \Omega' - \mu' \right) \right] \tilde{p}, \\ \tilde{u}_z &= -\frac{ik}{\rho\Lambda} \tilde{p}, \end{aligned} \quad (\text{A3})$$

where

$$\begin{aligned} E &= \Lambda^2 + \frac{2\Lambda\mu r}{\tilde{\lambda}_\eta\rho\mu_0} \left(\frac{iF}{\tilde{\lambda}_\eta} \Omega' - \mu' \right) + 2 \left(\Omega - \frac{i\mu F}{\tilde{\lambda}_\eta\rho\mu_0} \right) \\ &\quad \times \left[2\Omega + \left(1 + \frac{F^2}{\tilde{\lambda}_\eta^2\rho\mu_0} \right) r\Omega' - \frac{2i\mu F}{\tilde{\lambda}_\eta\rho\mu_0} \right]. \end{aligned} \quad (\text{A4})$$

Upon substitution from (A3) for \tilde{u}_r , \tilde{u}_θ , the continuity equation (5) produces a second-order differential equation for \tilde{p}

$$\begin{aligned} &\frac{d}{dr} \left(\frac{\Lambda}{\rho E} \frac{d\tilde{p}}{dr} \right) + \left[\frac{\Lambda}{rE\rho} - \frac{im}{E\rho} \left(1 + \frac{F^2}{\rho\mu_0\tilde{\lambda}_\eta^2} \right) \Omega' \right] \frac{d\tilde{p}}{dr} \\ &+ \frac{2im}{Er^2\rho} \left(\Omega - \frac{iF\mu}{\rho\mu_0\tilde{\lambda}_\eta} \right) \tilde{p} + \frac{d}{dr} \left[\frac{2im}{Er\rho} \left(\Omega - \frac{iF\mu}{\rho\mu_0\tilde{\lambda}_\eta} \right) \right] \tilde{p} \\ &- \frac{2m^2}{Er^2\rho} \left(\frac{\Lambda}{2} + \frac{\mu r}{\rho\mu_0\tilde{\lambda}_\eta} \left(\frac{iF}{\tilde{\lambda}_\eta} \Omega' - \mu' \right) \right) \tilde{p} - \frac{k^2}{\Lambda\rho} \tilde{p} = 0. \end{aligned} \quad (\text{A5})$$

The first of equations (A3) yields an expression for $\chi = -r\tilde{u}_r/\tilde{\lambda}_\eta$ in terms of \tilde{p} and $d\tilde{p}/dr$

$$\chi = \frac{\Lambda r}{\tilde{\lambda}_\eta E\rho} \frac{d\tilde{p}}{dr} + \frac{2im}{E\rho\tilde{\lambda}_\eta} \left(\Omega - \frac{iF\mu}{\rho\mu_0\tilde{\lambda}_\eta} \right) \tilde{p}. \quad (\text{A6})$$

In order to derive the equation for χ , first we take the radial derivative of (A6), and eliminate the second derivative of \tilde{p} , with the help of (A5), leaving

$$\begin{aligned} \frac{d\chi}{dr} &= \frac{im}{E\rho\tilde{\lambda}_\eta} \left[\left(1 - \frac{\tilde{\lambda}_\nu}{\tilde{\lambda}_\eta} \right) r\Omega' + 2 \left(\Omega - \frac{iF\mu}{\rho\mu_0\tilde{\lambda}_\eta} \right) \right] \frac{d\tilde{p}}{dr} \\ &+ \frac{2m^2}{E\rho\tilde{\lambda}_\eta^2} \left(\Omega - \frac{iF\mu}{\rho\mu_0\tilde{\lambda}_\eta} \right) \Omega' \tilde{p} \\ &+ \frac{h^2 r}{\Lambda E \rho \tilde{\lambda}_\eta} \left[\Lambda^2 + \frac{2\mu r}{\tilde{\lambda}_\eta \rho \mu_0} \Lambda \left(\frac{iF}{\tilde{\lambda}_\eta} \Omega' - \mu' \right) \right] \tilde{p} \\ &+ \frac{2k^2 r}{\Lambda E \rho \tilde{\lambda}_\eta} \left[2\Omega + \left(1 + \frac{F^2}{\tilde{\lambda}_\eta^2 \rho \mu_0} \right) r\Omega' - \frac{2i\mu F}{\tilde{\lambda}_\eta \rho \mu_0} \right] \\ &\times \left(\Omega - \frac{i\mu F}{\tilde{\lambda}_\eta \rho \mu_0} \right) \tilde{p}, \end{aligned} \quad (\text{A7})$$

where h is defined by (10). A combination of (A6) and (A7) brings the expression for $d\tilde{p}/dr$ in terms of χ and $d\chi/dr$

$$\begin{aligned} \frac{d\tilde{p}}{dr} &= -\frac{2i\rho m \tilde{\lambda}_\eta}{h^2 r^2} \left(\Omega - \frac{iF\mu}{\rho\mu_0\tilde{\lambda}_\eta} \right) \frac{d\chi}{dr} + \frac{\rho\tilde{\lambda}_\eta E}{\Lambda r} \chi \\ &- \frac{2\rho m^2 \tilde{\lambda}_\eta}{h^2 r^3 \Lambda} \left(\Omega - \frac{iF\mu}{\rho\mu_0\tilde{\lambda}_\eta} \right) \left[\left(1 - \frac{\tilde{\lambda}_\nu}{\tilde{\lambda}_\eta} \right) r\Omega' \right. \\ &\left. + 2 \left(\Omega - \frac{iF\mu}{\rho\mu_0\tilde{\lambda}_\eta} \right) \right] \chi. \end{aligned} \quad (\text{A8})$$

This helps us to rule out $d\tilde{p}/dr$ from (A7) and obtain

$$\begin{aligned} \Lambda r \frac{d\chi}{dr} - im \left[\left(1 - \frac{\tilde{\lambda}_\nu}{\tilde{\lambda}_\eta} \right) r\Omega' + 2 \left(\Omega - \frac{iF\mu}{\rho\mu_0\tilde{\lambda}_\eta} \right) \right] \chi \\ = \frac{h^2 r^2}{\rho\tilde{\lambda}_\eta} \tilde{p}. \end{aligned} \quad (\text{A9})$$

Multiplying both sides of (A9) by $\rho\tilde{\lambda}_\eta/(h^2 r^2)$, taking the derivative in r and then substituting from (A8) for $d\tilde{p}/dr$ expressed in terms of χ and $d\chi/dr$, we eventually arrive at the modified Hain-Lüst equation (11)

$$\frac{d}{dr} \left(f \frac{d\chi}{dr} \right) + s \frac{d\chi}{dr} - g\chi = 0, \quad (\text{A10})$$

supplemented by (12).

Appendix B: Hain-Lüst dispersion relation

We write again the dispersion relation (13), which we deduced from the extended Hain-Lüst equation (11)

$$\begin{aligned} &\tilde{\lambda}_\eta^2 \Lambda^2 + 4\alpha^2 \left(\Omega\tilde{\lambda}_\eta - \frac{iF\mu}{\rho\mu_0} \right) \\ &\times \left[\Omega Ro(\omega_\eta - \omega_\nu) + \left(\Omega\tilde{\lambda}_\eta - \frac{iF\mu}{\rho\mu_0} \right) \right] \\ &+ \frac{4\Lambda h^2 \tilde{\lambda}_\eta}{h^2 + q^2} \left[\left(\Omega^2 Ro - \frac{\mu^2}{\rho\mu_0} Rb \right) + \frac{imr}{2} \frac{d}{dr} \left(\frac{\Omega\tilde{\lambda}_\eta - \frac{i\mu F}{\rho\mu_0}}{h^2 r^2} \right) \right] \\ &= 0, \end{aligned} \quad (\text{B1})$$

where $\Lambda = \tilde{\lambda}_\nu + \frac{F^2}{\tilde{\lambda}_\eta \rho \mu_0}$ and $\alpha^2 = \frac{k^2}{h^2 + q^2}$. The dispersion relation in the work [21] differs from (B1) only by the term

$$\frac{4\Lambda h^2 \tilde{\lambda}_\eta}{h^2 + q^2} \frac{imr}{2} \frac{d}{dr} \left(\frac{\Omega\tilde{\lambda}_\eta - \frac{i\mu F}{\rho\mu_0}}{h^2 r^2} \right). \quad (\text{B2})$$

We illustrate the difference by calculating the growth rates given by the two dispersion relations for $Ro = -1/2$, $Rb = -1/2$, $m = 1$, and $Pm = 1$. We define α_1 by $\alpha_1^2 = k^2/(k^2 + q^2)$. Expanding the growth rates at large values of Ha_θ for (B1) with and without the term (B2), we find

$$\begin{aligned} \frac{\Re(\lambda)}{\Omega} &= a_H Ha_\theta + O(Ha_\theta^0), \\ \frac{\Re(\lambda)}{\Omega} &= a_K Ha_\theta + O(Ha_\theta^0), \end{aligned} \quad (\text{B3})$$

respectively, where

$$\begin{aligned} a_H &= \frac{1}{Re \sqrt{(1 + (rk)^2)(\alpha_1^2 + (rk)^2)}} \\ &\times \left\{ (\alpha_1^2 - 1)(rk)^2 - (1 + \alpha_1^2)(rk)^4 \right. \\ &+ \alpha_1 \left[4(rk)^4(1 + (rk)^2)^2 + \alpha_1^4(1 + 8(rk)^2 \right. \\ &\left. \left. + 10(rk)^4 + (rk)^8 \right) \right]^{\frac{1}{2}} \left. \right\}^{\frac{1}{2}}, \\ a_K &= \frac{1}{Re} \sqrt{\alpha_1^2(4 + \alpha_1^2) - (1 + \alpha_1^2)}. \end{aligned} \quad (\text{B4})$$

The relation between a_H and a_K becomes clear, if we expand a_H in power of $1/k$ at large values of $|k|$ leaving

$$\begin{aligned} a_H &= \frac{1}{Re} \sqrt{\alpha_1^2(4 + \alpha_1^2) - (1 + \alpha_1^2)} \\ &+ \frac{\left((3 + \alpha_1^2) \sqrt{\alpha_1^2(4 + \alpha_1^2) - \alpha_1^2(5 + \alpha_1^2)} \right) \sqrt{\alpha_1^2}}{2\sqrt{\alpha_1^2 + 4} \sqrt{\alpha_1^2(4 + \alpha_1^2) - 1 - \alpha_1^2} Re} \frac{1}{k^2 r^2} \\ &+ O\left(\frac{1}{k^4}\right). \end{aligned} \quad (\text{B5})$$

We find that the leading order term is a_K .

-
- [1] E. Velikhov, JETP (USSR) **36**, 1398 (1959).
- [2] S. Chandrasekhar, Proc. Natl. Acad. Sci. **46**, 253 (1960).
- [3] A. Balbus and J. F. Hawley, Astrophys. J. **376**, 214 (1991).
- [4] O. N. Kirillov and F. Stefani, Astrophys. J. **712**, 52 (2010).
- [5] O. N. Kirillov and F. Stefani, Acta Appl. Math. **120**, 177 (2012).
- [6] S. Friedlander and M. M. Vishik, Chaos **5**, 416 (1995).
- [7] G. I. Ogilvie and J. E. Pringle, Mon. Not. R. Astron. Soc. **279**, 152 (1996).
- [8] R. Zou and Y. Fukumoto, Prog. Theor. Exp. Phys. 113J01, (2014).
- [9] R. Hollerbach and G. Rüdiger, Phys. Rev. Lett. **95**, 124501 (2005).
- [10] R. Salmeron and M. Wardle, Mon. Not. R. Astron. Soc. **345**, 992 (2003).
- [11] F. Ebrahimi, B. Lefebvre, C. B. Forest and A. Bhattacherjee, Phys. Plasmas **18**, 062904 (2011).
- [12] M. Seilmayer, V. Galindo, G. Gerbeth, T. Gundrum, F. Stefani, M. Gellert, G. Rüdiger, M. Schultz and R. Hollerbach, Phys. Rev. Lett. **113**, 024505 (2014).
- [13] R. Hollerbach, V. Teeluck and G. Rüdiger, Phys. Rev. Lett. **104**, 044502 (2010).
- [14] G. Rüdiger, M. Gellert, M. Schultz, R. Hollerbach and F. Stefani, Mon. Not. R. Astron. Soc. **438**, 271 (2014).
- [15] A. Balbus and P. Henri, Astrophys. J. **674**, 408 (2008).
- [16] S. J. Desch, Astrophys. J. **608**, 509 (2004).
- [17] J. C. B. Papaloizou and C. Terquem, Mon. Not. R. Astron. Soc. **287**, 771 (1997).
- [18] A. Brandenburg, A. Nordlund, R. F. Stein and U. Torkelsson, Astrophys. J. **446**, 741 (1995).
- [19] C. Terquem and J. C. B. Papaloizou, Mon. Not. R. Astron. Soc. **279**, 767 (1996).
- [20] A. Balbus and J. F. Hawley, Astrophys. J. **392**, 662 (1992).
- [21] O. N. Kirillov, F. Stefani and Y. Fukumoto, Fluid Dyn. Res. **46**, 031403 (2014).
- [22] R. J. Tayler, Mon. Not. R. Astron. Soc. **161**, 365 (1973).
- [23] R. J. Tayler, Mon. Not. R. Astron. Soc. **191**, 151 (1980).
- [24] C. Curry and R. E. Pudritz, Mon. Not. R. Astron. Soc. **281**, 119 (1996).
- [25] J. Squire and A. Bhattacherjee, Phys. Rev. Lett., **113**, 025006 (2014).
- [26] O. N. Kirillov, F. Stefani and Y. Fukumoto, Astrophys. J. **712**, 52 (2012).
- [27] O. Kirillov and F. Stefani, Phys. Rev. E **92**, 051001 (2015).
- [28] O. N. Kirillov, Proc. R. Soc. A, 473(2205): 20170344 (2017).
- [29] O. N. Kirillov and F. Stefani, Phys. Rev. Lett. **111**, 061103 (2013).
- [30] O. N. Kirillov, F. Stefani and Y. Fukumoto, J. Fluid Mech., **760**, 591 (2014).
- [31] J. P. Goedbloed, R. Keppens and S. Poedts, *Advanced Magnetohydrodynamics* (Cambridge University Press. Cambridge, 2010).
- [32] J. P. Goedbloed and S. Poedts, *Principles of Magnetohydrodynamics* (Cambridge University Press. Cambridge, 2004).
- [33] A. P. Willis and C. F. Barenghi, Astron. & Astroph. **388**, 688–691 (2002).
- [34] O. N. Kirillov, D. E. Pelinovsky and G. Schneider, Phys. Rev. E **84**, 065301(R) (2011).
- [35] O. N. Kirillov and F. Stefani, Phys. Rev. E **84**(3), 036304 (2011).
- [36] W. Liu, J. Goodman, I. Herron and H. Ji, Phys. Rev. E **74**, 056302 (2006).
- [37] A. Child, E. Kersalé and R. Hollerbach, Math. Comput. **92**, 033011 (2015).
- [38] E. Frieman and M. Rotenberg, Rev. Mod. Phys. **32**, 898–902 (1960).
- [39] G. Rüdiger, R. Hollerbach, M. Schultz and D. Elstner, Mon. Not. R. Astron. Soc. **377**, 1481 (2007).
- [40] R. Hollerbach, Int. J. Num. Methods in Fluids **32**(7), 773–797 (2000).
- [41] K. Deguchi and M. Nagata, J. Fluid Mech. **678**, 156 (2011).
- [42] K. Deguchi, Phys. Rev. E **95**, 021102 (2017).
- [43] V. A. Vladimirov, H. K. Moffatt and K. I. Ilin J. Fluid Mech. **390**, 127–150 (1999).
- [44] K. Deguchi, J. Fluid Mech. **865**, 492–522 (2019).
- [45] G. Rüdiger and M. Schultz, Astron. Nachr. **331**, 121–129 (2010).
- [46] J. Priede, Phys. Rev. E **84**, 006314 (2011).
- [47] M. Seilmayer, F. Stefani, T. Gundrum, T. Weier, G. Gerbeth, M. Gellert and G. Rüdiger, Phys. Rev. Lett. **108**, 244501 (2012).
- [48] F. Stefani, A. Gailitis, G. Gerbeth, A. Giesecke, Th. Gundrum, G. Rüdiger, M. Seilmayer and T. Vogt, Geophys. & Astrophys. Fluid Dyn., **113**(1-2), 51–70 (2019).
- [49] G. Rüdiger, M. Gellert, R. Hollerbach, M. Schultz, F. Stefani, Physics Reports **741**, 1–89 (2018).
- [50] S. A. Balbus, Nature, **470**(7335), 475–476 (2011).
- [51] H. Ji and S. Balbus, Phys. Today, **66**, 27–33 (2013).
- [52] F. Stefani, T. Gundrum, G. Gerbeth, G. Rüdiger, M. Schultz, J. Szklarski and R. Hollerbach, Phys. Rev. Lett. **97**, 184502 (2006).
- [53] F. Stefani, G. Gerbeth, T. Gundrum, R. Hollerbach, J. Priede, G. Rüdiger and J. Szklarski, Phys. Rev. E **80**, 066303 (2009).
- [54] R. Hollerbach, G. Rüdiger and V. Teeluck, Phys. Rev. Lett. **104**, 044502 (2010).
- [55] W. Heinrichs, Math. Comput. **53**, 187 (1989).
- [56] G. Rüdiger, M. Gellert, M. Schultz and R. Hollerbach, Phys. Rev. E **82**, 1 (2010).
- [57] A. Guseva, A. P. Willis, R. Hollerbach and M. Avila, New J. Phys. **53**, 093018 (2015).